

Electron Spin Resonance of the Interacting Spinon Liquid

Kirill Yu. Povarov,^{1,*} Timofei A. Soldatov,² Ren-Bo Wang,³
Andrey Zheludev,¹ Alexander I. Smirnov,^{2,†} and Oleg A. Starykh^{3,‡}

¹*Laboratory for Solid State Physics, ETH Zürich, 8093 Zürich, Switzerland*

²*P. L. Kapitza Institute for Physical Problems RAS, 119334 Moscow, Russia*

³*Department of Physics and Astronomy, University of Utah, Salt Lake City, Utah 84112, USA*[†]

(Dated: August 9, 2021)

Quasiparticles of the Heisenberg spin-1/2 chain - spinons - represent the best experimentally accessible example of fractionalized excitations known to date. Dynamic spin response of the spin chain is typically dominated by the broad multi-spinon continuum that often masks subtle features, such as edge singularities, induced by the interaction between spinons. This, however, is not the case in the small momentum region of the magnetized spin chain where strong interaction between spinons leads to *qualitative* changes to the response. Here we report experimental verification of the recently predicted collective modes of spinons in a model material $K_2CuSO_4Br_2$ by means of the electron spin resonance (ESR). We exploit the unique feature of the material - the uniform Dzyaloshinskii-Moriya interaction between chain's spins - in order to access small momentum regime of the dynamic spin susceptibility. By measuring interaction-induced splitting between the two components of the ESR doublet we directly determine the magnitude of the marginally irrelevant backscattering interaction between spinons for the first time. We find it to be in an excellent agreement with the predictions of the effective field theory. Our results point out an intriguing similarity between the one-dimensional interacting liquid of neutral spinons and the Landau Fermi liquid of electrons.

Much of the current research in quantum magnetism is motivated by the search for an elusive quantum spin liquid (QSL) phase of the magnetic matter. A salient feature of this entangled quantum state is the presence of fractionalized elementary excitations such as fermionic spin-1/2 spinons, interactions between which are mediated by the emergent gauge field. This exotic perspective represents striking contrast with the usual interger-spin bosonic excitations, spin waves or magnons, of the magnetically ordered media. Yet this ‘radical’ point of view is deeply rooted in history. The *first* model of the quantum magnetism, solved by Bethe in 1931 [1], — antiferromagnetic spin-1/2 Heisenberg chain — has the spin liquid ground state (a filled one-dimensional Fermi ‘sphere’) and fractionalized spinon excitations obeying Pauli exclusion principle (although the full understanding of this took a long time to develop [2]). This dramatic beginning was followed by Pomeranchuk’s proposal that an antiferromagnet realizes a liquid of neutral fermions [3, 4] and culminated with Anderson’s resonating valence bond idea [5] which underlies the modern QSL quest [6]. The theoretical efforts were accompanied by remarkable experimental findings on (quasi) one-dimensional (1D) spin-1/2 magnetic insulators. These include observations of particle-hole continuum of excitations (also referred to as a “two-spinon continuum”) in the inelastic neutron scattering experiments [7] and magnetic field-controlled soft modes resulting from transitions on the Zeeman-split 1D Fermi surfaces [8, 9]. The most recent milestone of this journey is provided by the Kitaev’s honeycomb model which harbors Majorana fermions as elementary excitations [10]. Experimental glimpses of this exciting physics, via the Fermi-Dirac-like Raman scattering background [11] and approximately quantized thermal Hall conductivity in α -RuCl₃ [12, 13], continue to attract intense attention of

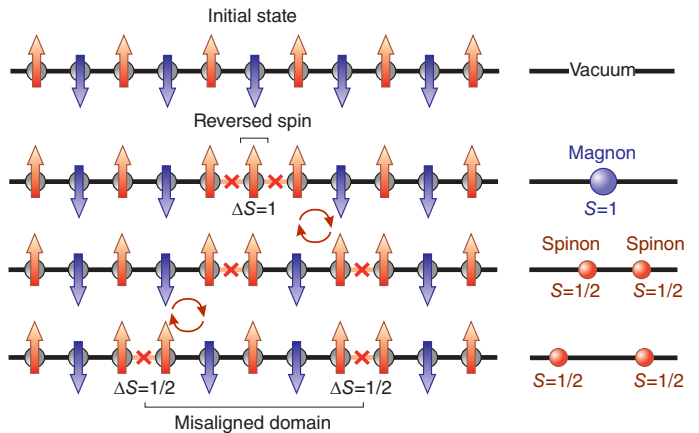


FIG. 1. **Fractionalization of excitations in one-dimensional antiferromagnets.** Left: cartoon shows how a single flipped spin in a 1D antiferromagnetic chain ‘breaks’ into two domain walls at no energy cost. The total spin of the state remains 1 and the amount of broken bonds (red crosses) is always two. Right: the same process in the quasiparticle language. The antiferromagnetic state corresponds to the vacuum with no particles present, and a flipped spin corresponds to a single $S = 1$ magnon excitation. Subsequently this particle decays into a pair of $S = 1/2$ spinon excitations.

the scientific community.

Close analogy between fractionalized excitations of the QSL and those of the standard Fermi liquid contains an important caveat. Unlike the latter, elementary excitations of the QSL are highly non-local objects. For example, in the Ising limit of the spin-1/2 chain a spinon can be visualized as a kink (domain wall) separating two opposite Néel domains. Therefore such an excitation can not be represented by any finite number of local spin

operators. A corollary to that is that every local spin operator (say, that of a spin flip \hat{S}^-) always creates an *even* number of quasiparticles (2 or 4 or more), as illustrated in Fig. 1. This familiar picture points out the importance of interactions between fractionalized quasi-particles: spinons which appear and disappear only in pairs can not avoid interacting with each other.

In more technical terms, spin operators are expressed via bilinear combinations of spinons and, as a result, dynamical spin susceptibility is determined by the spinon particle-hole continuum which is well documented experimentally [7, 9, 14]. Interaction between spinons, as well as the curvature of the spinon dispersion, determine shape of the continuum near its edges [15, 16]. The interaction becomes most important when magnetic field is applied — it shifts spinon continuum up in energy and produces a spin-1 oscillatory collective mode of spinons [17], originating from the Larmor frequency, a spin chain analog of the Silin's spin wave in conductors [18–22].

In this paper we, for the first time, experimentally investigate this interaction-induced modification of the spinon continuum with the help of the electron spin resonance (ESR) technique. Our measurements lead to the unambiguous determination of the backscattering interaction between fractionalized spinon excitations of the spin chain. This finding is facilitated by the unique feature of the material — the uniform Dzyaloshinskii–Moriya (DM) interaction [23, 24], direction and magnitude of which are also determined experimentally, that turns the ESR measurement into a finite momentum probe of the dynamic spin susceptibility.

The material of our study is bromotinoite $K_2CuSO_4Br_2$, a synthetic analogue of the natural mineral chlorotionite [26]. It provides an outstanding realization of the $S = 1/2$ Heisenberg chain antiferromagnet perturbed by a small uniform DM interaction \mathbf{D} [27–29]. The presence of the spinon continuum was directly confirmed through the inelastic neutron scattering studies of $K_2CuSO_4Br_2$ [27, 28]. A sketch of the crystal structure is shown in the inset of Fig. 2a. The magnetic Cu^{2+} spin-1/2 ions are forming linear chains running along the \mathbf{a} axis of the orthorhombic P_{nma} crystal structure. The distance between the magnetic ions is $a = 7.73$ Å. Antiferromagnetic interaction $J \simeq 20.5$ K [27] is mediated by a two-bromine unit, that lacks inversion center within the ac plane. This lack of inversion symmetry naturally gives rise to the DM interaction $\mathbf{D} = (0, D, 0)$ directed along the b axis of the crystal. A *uniform*, bond-independent arrangement of DM vectors within the chain is a very rare occasion. However, a truly remarkable property of $K_2CuSO_4Br_2$ that distinguishes it from similar materials (e.g. Cs_2CuCl_4 [30, 31]) is that the DM axis is the *same*, i.e. oriented along the b crystal axis, for all spin chains [27]. The DM vector is a single-component one, the sign of its b component alternates $\pm D$ between neighboring chains while its two other components are

zero. This unique feature makes it possible to apply external magnetic field exactly along the DM vector, which is a crucial element of our study.

Denoting the common $\mathbf{D} \parallel \mathbf{H}$ axis as z -axis, the Hamiltonian of the chain with $\mathbf{D} = (0, -D, 0)$ reads

$$\hat{\mathcal{H}} = \sum_n J \hat{\mathbf{S}}_n \cdot \hat{\mathbf{S}}_{n+1} - D (\hat{\mathbf{S}}_n \times \hat{\mathbf{S}}_{n+1})_z - g\mu_B H \hat{S}_n^z. \quad (1)$$

Semiclassically, the competition between the Heisenberg exchange J (that forces the neighboring spins to be antiparallel) and DM interaction \mathbf{D} (that forces them to be perpendicular) results in an incommensurate spiral, period of which is determined by the wavevector $q_{DM} = a^{-1}D/J$. This implies that in the twisted reference frame that rotates by angle $\arctan(D/J)$ around the z -axis between neighboring sites, the spiraling pattern of spins turns into the collinear one. Quantum-mechanically, this transformation corresponds to the unitary position-dependent rotation of spins which eliminates $\mathbf{D} \cdot \hat{\mathbf{S}}_n \times \hat{\mathbf{S}}_{n+1}$ term from the Hamiltonian (1) [25, 32]. Simultaneously, it shifts the wavevector by q_{DM} . Despite being small, this shift is of utmost importance for the ESR response of the chain.

The ESR, which measures rate of absorption of the microwave radiation (with mm-range wavelength) by the crystal, is determined by the imaginary part of the transverse spin susceptibility, $\chi''(0, \nu)$. The above argument about the DM-induced shift shows that in a spin chain with uniform DM interaction and magnetic field parallel to it (1), the energy absorption rate is instead determined by $\chi''(q_{DM}, \nu)$ [32, 33] — the ESR becomes a finite momentum probe of the dynamic spin susceptibility!

To explore the physical consequences of this remarkable observation, we need to introduce effective fermion description of (1) [17, 34–36] (which is strictly equivalent to the standard bosonization approach [37, 38] but is better suited for our analysis). In the low-energy continuum limit $\hat{\mathcal{H}} \rightarrow \hat{\mathcal{H}}_0 + \hat{V}_{bs}$, which are compactly expressed via two component spinors $\hat{\psi}_{R/L} = (\hat{\psi}_{R/L,\uparrow}, \hat{\psi}_{R/L,\downarrow})^T$ and spin current (uniform spin density) operators $\hat{\mathbf{J}}_{R/L} = \frac{1}{2} \hat{\psi}_{R/L}^\dagger \boldsymbol{\sigma} \hat{\psi}_{R/L}$ (see [25])

$$\hat{\mathcal{H}}_0 = \int dx \left[\hbar v_F \left(\hat{\psi}_R^\dagger(x) (-i\partial_x) \hat{\psi}_R(x) + \hat{\psi}_L^\dagger(x) (i\partial_x) \hat{\psi}_L(x) \right) - g\mu_B H \left(\hat{J}_R^z(x) + \hat{J}_L^z(x) \right) \right], \quad (2)$$

$$\hat{V}_{bs} = -\hbar u \int dx \hat{\mathbf{J}}_R(x) \cdot \hat{\mathbf{J}}_L(x). \quad (3)$$

Here $v_F = \pi Ja/(2\hbar)$ is the spinon velocity, and u denotes backscattering (current-current) interaction between spinons. Operators $\hat{\psi}_{R/L,s}$ describe spin- s fermions with wavevectors near the right/left Fermi points $\pm k_{F,s}$ of the 1D Fermi surface (see [25]).

Despite its somewhat complicated appearance $\hat{\mathcal{H}}_0$ describes a non-interacting gas of neutral fermions

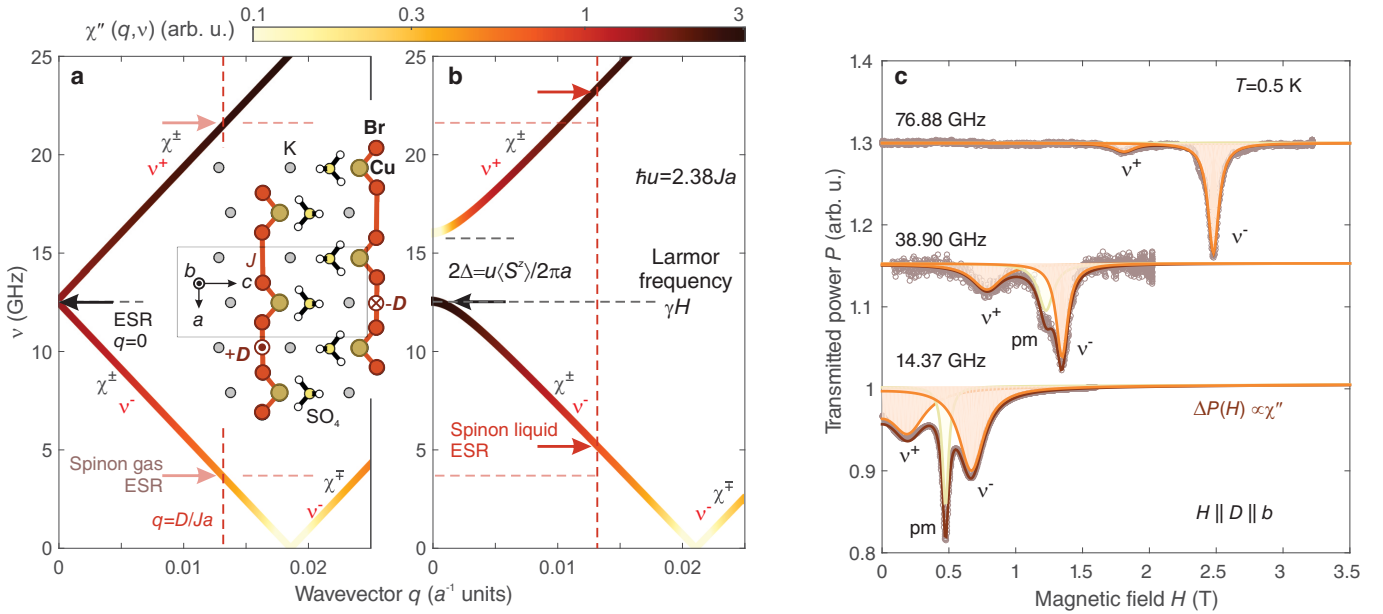


FIG. 2. Electron spin resonance in $\text{K}_2\text{CuSO}_4\text{Br}_2$: theoretical and experimental. **a**, Calculated spectrum of small- q transverse spin fluctuations in a magnetized spin chain without the backscattering interaction. **b**, The same for the interacting spinons, $\hbar\nu = 2.38Ja$. For $\text{K}_2\text{CuSO}_4\text{Br}_2$ considered here $J = 20.5$ K, and the magnetic field is 0.3 T in both panels. The solid lines show $\nu(q)$ for the poles of the transverse spin susceptibility according to Ref. [17] (see [25] for more details), and the color shows their intensity. Black (red) horizontal arrows indicate resonance frequencies of the spin chain without (black) and with (red) the DM interaction. The inset shows an *ac* plane projection of $\text{K}_2\text{CuSO}_4\text{Br}_2$ crystal structure with the Cu-Br-Br-Cu chains running along a and the DM vectors pointing along b (the two-fold rotation axis of the structure). **c**, Several low- T resonance lines in $\text{K}_2\text{CuSO}_4\text{Br}_2$. Magnetic field is applied along the DM axis $D \parallel b$. The measured rate of absorption of the microwave radiation by the sample (gray points) is the direct probe of the dissipative susceptibility. It is well fitted by several Lorentzian lines (dark red line). The contributions of modes ν^+ and ν^- is shown in orange color. At low frequencies an additional parasitic paramagnetic resonance can be detected (light green color).

(spinons) $\psi_{R/L,s}$, subject to the external magnetic field. For the sake of brevity we present (2) and (3) with $D = 0$ here, see [25] for the general formulation. Interaction between spinons is compactly encoded in \hat{V}_{bs} , which describes scattering of right- and left-moving fermions on each other. The amplitude u of this $2k_F$ backscattering, which includes both spin-flip and non-spin-flip processes, is, in fact, a *running* coupling constant. Due to the dependence on spinon distribution functions, this marginally irrelevant interaction is a weak function of the temperature T and magnetic field H , vanishing in the limit $T, H \rightarrow 0$. Quantitatively, this dependence is described by the Renormalization Group (RG) technique [37, 39, 40].

Basic understanding of the ESR response of the *ideal* spin chain, Eq.(1) with $D = 0$, follows from the *non-interacting* $\hat{\mathcal{H}}_0$ [41]. Imaginary part of the transverse spin susceptibility $\chi^\pm(q, \omega)$ of the magnetized chain defines a two-spinon continuum with a characteristic wedge-like shape in the $q-\nu$ plane, illustrated in Fig. 2a. At exactly $q = 0$ the continuum collapses to a point, a single resonance frequency $\hbar\nu = g\mu_B H$, as required by the Larmor theorem. For any $q \neq 0$ there are *two* distinct resonance frequencies, at $g\mu_B H \pm \hbar\nu_F q$, describing contributions from right- and left-moving spinons, correspondingly

[25, 41]. In addition, for a sufficiently large wavevector, there also is a contribution from the χ^\mp component of the susceptibility, at $\hbar\nu = \hbar\nu_F q - g\mu_B H$.

Our simple wavevector-shift argument, $q = 0 \rightarrow q = q_{\text{DM}}$, presented above, suggests that the ESR spectrum of the spin chain with *finite* DM, as given by the *full* Eq. (1), is described by the ESR *doublet* [32]

$$\hbar\nu^\pm = |g\mu_B H \pm \frac{\pi}{2}D|, \quad (4)$$

where we used $\hbar\nu_F q_{\text{DM}} = \pi D/2$, and also accounted for both χ^\pm and χ^\mp components of the susceptibility. Notice that obtained frequencies ν^\pm do not depend on the sign of D in (1), chains with $\mathbf{D} = (0, -D, 0)$ and $\mathbf{D} = (0, D, 0)$ contribute equally to the ESR response.

The appearance of the ESR doublet in the quantum spin liquid state of the spin chain is the fingerprint of the uniform DM. It has been experimentally observed previously in three different materials, Cs_2CuCl_4 [31], the present compound $\text{K}_2\text{CuSO}_4\text{Br}_2$ [42], and $\text{K}_2\text{CuSO}_4\text{Cl}_2$ [43].

However, the non-interacting spinon description of the dynamic spin response is qualitatively incomplete. Main findings of the recent interacting spinon theory [17] can be summarized as follows (see [25] for more details). Similar to the case of the interacting electron liquid [18, 19],

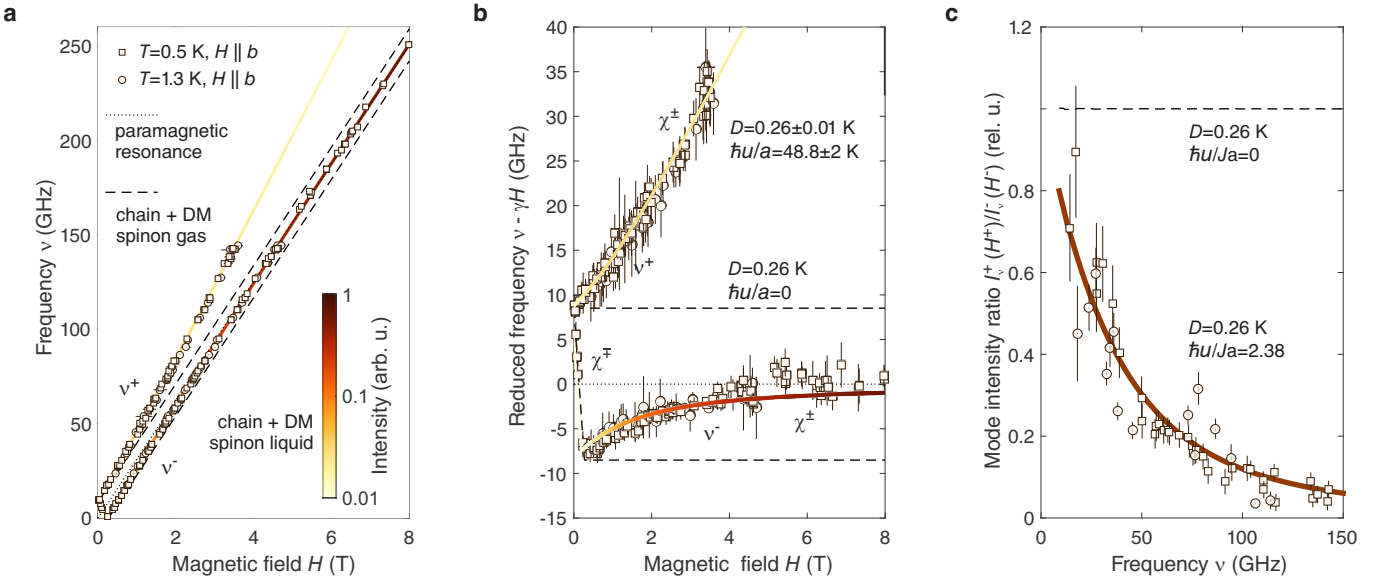


FIG. 3. ESR spectrum of $\text{K}_2\text{CuSO}_4\text{Br}_2$ and its theoretical description in terms of interacting spinons. **a**, The frequency-field diagram including the $H \parallel D$ data at two different temperatures (circles and squares). Error bars are obtained from the lineshape fit and for the majority of ESR lines are estimated as 0.02 T and are within the symbol size. For some of frequencies above 50 GHz, the lineshape was distorted by the parasitic electrodynamic size effect, here errors in H -value are estimated as a whole linewidth and are seen as error bars on the left and middle panels. The dotted line is the $\hbar\nu = g\mu_B H$ paramagnetic resonance, the dashed lines correspond to the non-interacting approximation (4) with $D = 0.26$ K. The solid lines and their color (intensity, as indicated in the inset) correspond to the interacting spinon theory (5). The best-fit value of $\hbar u/a = 48.8$ K is used. **b**, The same diagram, but in the “reduced” representation with γH subtracted, $\nu \rightarrow \nu - \gamma H$. **c**, The mode intensity ratio versus the observation frequency. Points are the experimental data (as in the other panels), error bars stem from the experimental uncertainty in determining the widths and amplitudes of the two overlapping peaks. Solid line is the theoretical prediction (8) for the obtained best-fit value $\delta = 0.12$. The dashed line shows non-interacting spinons result.

residual backscattering interaction u between spinons qualitatively changes transverse spin susceptibility for small (q, ν) . Poles of $\chi^{\pm, \mp}$ are now given by [17, 25]

$$h\nu^{\pm} = \left| g\mu_B H + \Delta \pm \sqrt{\Delta^2 + (1 - \delta^2) \left(\frac{\pi}{2} D \right)^2} \right|. \quad (5)$$

Here $\Delta = \hbar u \langle \hat{S}^z \rangle / 2a$ is the interaction-induced spectral gap (splitting) and $\langle \hat{S}^z \rangle / a = \chi H$ is the spin z -component per unit length. The theory is most compactly expressed in terms of the small dimensionless parameter δ ,

$$\delta = \frac{1}{2a} \hbar u \frac{\chi_0}{g\mu_B} = \frac{u}{4\pi v_F}, \quad (6)$$

that describes the enhancement of the renormalized zero-field spin susceptibility per unit length $\chi = \chi_0 / (1 - \delta)$, from its non-interacting value $\chi_0 = g\mu_B a / (2\pi\hbar v_F)$. Using δ , the interaction-induced splitting becomes:

$$\Delta = \frac{\delta}{1 - \delta} g\mu_B H. \quad (7)$$

Even when $D = 0$, Eq.(5) predicts finite spectral gap 2Δ between the ν^{\pm} branches, as Fig. 2b shows. (This splitting has been seen previously in the numerical Bethe-ansatz study [44].) This finding does not contradict

the Larmor theorem because the intensity of the upper branch ν^+ vanishes as q^2 in the $q \rightarrow 0$ limit, whereas the lower intense branch ν^- remains exactly at the Larmor frequency $h^{-1}g\mu_B H = \gamma H$. Hence, in absence of the symmetry-breaking perturbations the Larmor theorem is obeyed, and backscattering interaction u makes no difference for the ESR experiment.

However, the uniform DM interaction in (1) is exactly the symmetry breaking one. The DM-induced wavevector shift by q_{DM} , which leads to the second term under the square-root in (5), makes both modes visible. Simultaneously, the interaction-induced gap Δ strongly modifies the frequency-field dependence (5) and makes deviations from the simple linear form obvious, as can be seen in Fig. 2b.

To compare these predictions with the ESR experiments on $\text{K}_2\text{CuSO}_4\text{Br}_2$ we use two sets of data. One, taken at $T = 0.5$ K, was previously partly described in [42]. The other set, taken at $T = 1.3$ K, was not presented before. The datasets involve multiple samples of $\text{K}_2\text{CuSO}_4\text{Br}_2$. The experiments were done at the Kapitza Institute (Moscow) on a set of multifrequency (1–250 GHz) resonant cavity ESR inserts into ${}^3\text{He}$ -pumping cryostat with a 14 T cryomagnet and a ${}^4\text{He}$ -pumping cryostat with a 6 T magnet.

The transmission of the microwave radiation through

the sample containing cavity P is affected by the dissipative susceptibility of the spin subsystem and can be approximately expressed as $\Delta P/P \propto \chi''(0, \nu)$, or rather $\chi''(q_{\text{DM}}, \nu)$ in the presence of the uniform DM interaction. Several examples of the raw spectrometer microwave transmission data at 0.5 K are shown in Fig. 2c. The data demonstrates a well-resolved doublet of ν^{\pm} lines, with a parasitic line in the middle that comes from impurities and is sample-dependent in intensity. It shows that the relative intensity of ν^+ line is strongly reduced at higher frequency.

This observation can be further quantified by fitting measured ESR spectra with three Lorentzian functions, keeping the line centers, full widths at half maxima, and amplitudes as fitting parameters. Results of this new data analysis are presented in Fig. 3: the positions of the lines vs frequency are shown in panels a and b, and the line intensity ratios vs frequency – in the panel c.

The deviation between the data and the non-interacting spinon approximation (4) is clearly visible in the frequency-field diagrams of Fig. 3a,b. The mode ν^+ , corresponding to the plus sign in (4), (5), strongly shifts up in frequency while rapidly loosing the intensity at the same time. The mode ν^- remains intense and instead quickly approaches the Larmor frequency. For the field above 4 T (frequency above 150 GHz) the paramagnetic resonance is essentially restored.

While being completely unexplainable within the previous non-interacting approximation (4), both effects – the upward deflection and the fading of the upper ν^+ mode and the restoration of the Larmor precession for the lower ν^- mode – are readily explained by the new interacting spinon expression (5). The upward shift of the ν^+ mode is the consequence of the gap Δ (7) growing with the field. The same effect is responsible for the upward approach of the ν^- mode towards the Larmor frequency, as is seen in Fig. 3.

Fitting the $\nu(H)$ data to Eq.(5), we find an excellent agreement between the experiment and the interacting-spinon theory for the value $\delta = 0.12 \pm 0.005$. By Eq.(6), this means that the backscattering interaction constant is $\hbar u/a = 48.8 \pm 2$ K. This is a strong interaction indeed, it corresponds to 2.38 ± 0.1 in the exchange coupling J units. What matters, however, is that u enters equations (5) and (7) only via δ , which is quite small. This smallness implies the consistency of the made theoretical assumptions. (This is further confirmed by the spinon mean-free path estimate in Sec. VII of the SM [25].) Note that DM interaction strength D , while being an independent parameter of the fit, is actually unchanged compared to the previous estimate 0.26 ± 0.01 K [42]. Its value is fixed by the zero field splitting $\pi D/2$ which at zero magnetization is not affected by the interaction u .

Direct comparison of the experimental intensities of ν^{\pm} modes with the theory [17] is unfeasible: there is no absolute calibration for the microwave susceptibility measurements by the used ESR spectrometers, and the response to microwave susceptibility χ'' itself is different

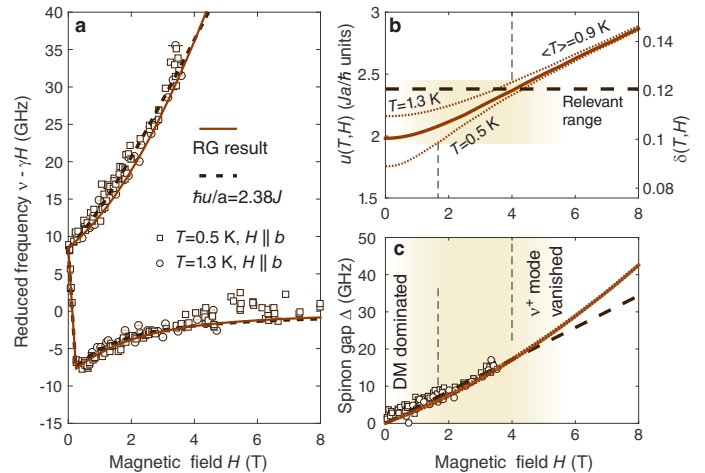


FIG. 4. Constant backscattering versus running coupling approach. **a**, The “reduced” frequency-field diagram comparing the best fit from Fig. 3b with the exact RG equation (9), shown by dashed and solid lines correspondingly. We have removed error bars from the data points here in order to highlight the difference between the two theoretical fits. The RG result gives a good qualitative description, but the systematic deviations from the data are noticeable. **b**, The running backscattering interaction parameter $u(H, T)$ at different relevant temperatures (solid and dotted lines) compared to the constant u best-fit value (horizontal dashed line). Shading and the vertical lines delineate the field region that affects the fit the most. The obtained value of u is close to the upper boundary of the RG result. **c**, Spinon gap Δ (7) for the same approaches as in the panel (a) above, and also the experimental value extracted from the spectra ($\Delta = \frac{\hbar}{2}(\nu^+ - \nu^-) - \gamma H$). In practice the impact of temperature turns out to be minor. In addition, this gap is smaller than the magnitude of the DM interaction (and hence $H = 0$ gap) for fields less than 2 T. Above 4 T, the ν^+ mode that is most sensitive to Δ , loses its intensity.

for different cavity resonance frequencies. However, this difficulty is easily avoided when we look at the *intensity ratio* $I_{\nu}^+(H^+)/I_{\nu}^-(H^-)$ at a fixed frequency ν (with H^{\pm} being the resonant fields of the corresponding modes). All the unknown factors are cancelled this way, and the experiment can be directly compared to theory which predicts (see [25])

$$\frac{I_{\nu}^+(H^+)}{I_{\nu}^-(H^-)} = \frac{\sqrt{(h\nu\delta)^2 + ((1 - \delta^2)\pi D/2)^2} - h\nu\delta}{\sqrt{(h\nu\delta)^2 + ((1 - \delta^2)\pi D/2)^2} + h\nu\delta}. \quad (8)$$

This parameter-free comparison is shown in Fig. 3c. We find an excellent agreement between all our datasets and the theory (8) for the derived value $\delta = 0.12$. Notice that without the backscattering interaction u , i.e. for $\delta = 0$, the ratio would be just 1 for all frequencies. Thus, the relative attenuation of the ν^+ mode represents an additional confirmation of the validity of the interacting spinon description of $\text{K}_2\text{CuSO}_4\text{Br}_2$.

How does the obtained value of u compare to the theoretical expectations? This is a rather nontrivial question

as according to the RG the backscattering interaction constant is actually a *running* one. The dependence of δ (and hence, u (6)) on the field and temperature is expressed via the following RG flow equation [45, 46]

$$\frac{1}{2\delta} + \frac{\ln 2\delta}{2} = \ln \left(\sqrt{\frac{\pi}{2}} e^{1/4} \frac{J}{T} \right) - \text{Re} \left[\psi \left(1 + i \frac{g\mu_B H}{2\pi T} \right) \right], \quad (9)$$

where $\psi(x) = \Gamma'(x)/\Gamma(x)$ is the digamma function. This equation implies that the positions of the ν^\pm modes should weakly depend on temperature for a fixed frequency of the spectrometer. However, we do not see much difference between the datasets at 1.3 and 0.5 K. The exact RG result (9) with *no* adjustable parameters (but using $\langle T \rangle = 0.9$ K as an ‘average’ value) is compared with the data and the constant- u fit in Fig. 4a. While it provides very convincing qualitative description of the data, on a closer look one finds small but systematic deviations for the ν^+ branch. The spinon gap Δ plotted versus field for the RG approach (Fig. 4c) shows virtually no change between the relevant temperatures. This is due to the magnetization being very small in the region that is sensitive to the effect of temperature. The corresponding plot of $u(H, T)$ is shown in Fig. 4b. In addition, the spinon gap Δ remains small compared to the zero-field gap $\pi D/2$ up to almost 2 T. This means that this region is less sensitive to the details of u behavior. Notice that the small magnitude of D is important for making this field interval smaller. Another insensitive region occurs above 4 T when the ν^+ mode becomes unobservable. This leaves us with a narrow region between 2 and 4 T, where the difference between the RG-based and the constant- u approaches is quite small yet visible.

Both the temperature T and the Zeeman energy $g\mu_B H$ in our experiment are small, but not *very* small compared to J . In addition, some other small energy scales unaccounted for in (9) may be at play, such as the interchain interaction or the finite-size effects due to the impurities. This makes unambiguous detection of the RG flow of u impossible. The experimentally found constant best-fit value of $\hbar u/a \simeq 2.38J$ is close to the upper limit of the RG result. This value is also very close to the one derived from the exact diagonalization of the spin-1/2 Heisenberg chain [47] (note that there $\hbar u/a = 2\pi\lambda_0 = 2.27J$).

We therefore conclude the obtained best-fit value of u represents experimental determination of the *bare*, or the initial, value of the backscattering interaction in the Hamiltonian (3). This situation is truly unique and qualitatively different from previous observations of the backscattering interaction in spin-1/2 chains, via low- T behavior of the uniform spin susceptibility [48]

and nuclear magnetic relaxation rates measurements in Sr_2CuO_3 [49]. In these experimental probes the interaction manifests itself via a weak $\ln(\Lambda/T)$ dependences [39, 50, 51] in which the bare value of u enters only in the under-the-log high-energy cut-off Λ .

To summarize, the observed field induced evolution of the gaps between ESR-doublet components and Larmor frequency is very well fit by the model of interacting spinons. The backscattering interaction turns out to be a crucial ingredient for the *quantitative* description of the data. The obtained value of the spinon backscattering interaction $u \simeq 1.5v_F \simeq 3.5 \cdot 10^5$ cm/s is of the order of spinon velocity v_F , consistent with the values of the exchange integral and lattice constant determined in previous experiments. Further, the experimentally observed frequency dependence of relative intensity of the doublet components, reflecting spectral densities of the collective Larmor mode and the upper boundary of the two-spinon continuum, is also well described by the interacting theory.

Our finding confirms the fundamental concept of interacting fractionalized quasiparticles – spinons – as the basic feature of the ground state of the $S = 1/2$ Heisenberg antiferromagnetic chain. Experimental confirmation of the importance of interactions between spinons reveals a genuine Fermi-liquid-like (in contrast to a Fermi-gas-like) behavior of the quasiparticles constituting the ground state. Dynamic small-momentum response of the quantum spin chain demonstrates an amazing similarity with an electron liquid and, in particular, Silin spin waves in non-ferromagnetic conductors. This result paves way to spectroscopic investigations of more complex quantum spin liquids, including higher-dimensional ones [52, 53].

ACKNOWLEDGMENTS

The work at ETH Zürich has been supported by the SNSF Division II. We would like to thank Dr. Manuel Hälg and Dr. Wolfram Lorenz for their involvement at the early stage of the project. The work of R.B.W. and O. A. S. is supported by the National Science Foundation CMMT program under Grant No. DMR-1928919. The work at Kapitza Institute (experiments, data processing and data analysis) has been supported by the Russian Science Foundation Grant No. 17-12-01505. O.A.S. would like to thank Anna Keselman and Leon Balents for the collaboration on the interacting spinons project which helped him to get through the covid lockdown and provided theoretical foundation for the current investigation.

* poverovk@phys.ethz.ch

† smirnov@kapitza.ras.ru

‡ starykh@physics.utah.edu

¹ H. Bethe, “Zur Theorie der Metalle,” *Zeitschrift für Physik* **71**, 205–226 (1931).

² L.D. Faddeev and L.A. Takhtajan, "What is the spin of a spin wave?" *Physics Letters A* **85**, 375–377 (1981).

³ I. Pomeranchuk, "The thermal conductivity of the paramagnetic dielectrics at low temperatures," *J. Phys. USSR (JETP)* **4**, 357–374 (1941).

⁴ I. Dzyaloshinskii, "High T_c superconductivity: band electrons vs. neutral fermions," *Physica Scripta* **T27**, 89–95 (1989).

⁵ P. W. Anderson, "Resonating valence bonds: A new kind of insulator?" *Materials Research Bulletin* **8**, 153 – 160 (1973); "The Resonating Valence Bond State in La₂CuO₄ and Superconductivity," *Science* **235**, 1196–1198 (1987).

⁶ Lucile Savary and Leon Balents, "Quantum spin liquids: a review," *Reports on Progress in Physics* **80**, 016502 (2017).

⁷ D. Alan Tennant, Roger A. Cowley, Stephen E. Nagler, and Alexei M. Tsvelik, "Measurement of the spin-excitation continuum in one-dimensional KCuF₃ using neutron scattering," *Phys. Rev. B* **52**, 13368–13380 (1995).

⁸ D. C. Dender, P. R. Hammar, Daniel H. Reich, C. Broholm, and G. Aeppli, "Direct Observation of Field-Induced Incommensurate Fluctuations in a One-Dimensional $S = 1/2$ Antiferromagnet," *Phys. Rev. Lett.* **79**, 1750–1753 (1997).

⁹ M. B. Stone, D. H. Reich, C. Broholm, K. Lefmann, C. Rischel, C. P. Landee, and M. M. Turnbull, "Extended Quantum Critical Phase in a Magnetized Spin- $\frac{1}{2}$ Antiferromagnetic Chain," *Phys. Rev. Lett.* **91**, 037205 (2003).

¹⁰ Alexei Kitaev, "Anyons in an exactly solved model and beyond," *Annals of Physics* **321**, 2–111 (2006).

¹¹ Yiping Wang, Gavin B. Osterhoudt, Yao Tian, Paige Lampen-Kelley, Arnab Banerjee, Thomas Goldstein, Jun Yan, Johannes Knolle, Huiwen Ji, Robert J. Cava, Joji Nasu, Yukitoshi Motome, Stephen E. Nagler, David Mandrus, and Kenneth S. Burch, "The range of non-Kitaev terms and fractional particles in α -RuCl₃," *npj Quantum Materials* **5**, 14 (2020).

¹² Y. Kasahara, T. Ohnishi, Y. Mizukami, O. Tanaka, Sixiao Ma, K. Sugii, N. Kurita, H. Tanaka, J. Nasu, Y. Motome, T. Shibauchi, and Y. Matsuda, "Majorana quantization and half-integer thermal quantum Hall effect in a Kitaev spin liquid," *Nature (London)* **559**, 227–231 (2018), arXiv:1805.05022 [cond-mat.str-el].

¹³ J. A. N. Bruin, R. R. Claus, Y. Matsumoto, N. Kurita, H. Tanaka, and H. Takagi, "Robustness of the thermal Hall effect close to half-quantization in a field-induced spin liquid state," arXiv e-prints , arXiv:2104.12184 (2021), arXiv:2104.12184 [cond-mat.str-el].

¹⁴ Martin Mourigal, Mechthild Enderle, Axel Klöpperpieper, Jean-Sébastien Caux, Anne Stunault, and Henrik M. Rønnow, "Fractional spinon excitations in the quantum Heisenberg antiferromagnetic chain," *Nature Physics* **9**, 435–441 (2013).

¹⁵ Rodrigo G. Pereira, Steven R. White, and Ian Affleck, "Exact Edge Singularities and Dynamical Correlations in Spin-1/2 Chains," *Physical Review Letters* **100** (2008), 10.1103/physrevlett.100.027206.

¹⁶ Adilet Imambekov, Thomas L. Schmidt, and Leonid I. Glazman, "One-dimensional quantum liquids: Beyond the Luttinger liquid paradigm," *Reviews of Modern Physics* **84**, 1253–1306 (2012).

¹⁷ A. Keselman, L. Balents, and O. A. Starykh, "Dynamical Signatures of Quasiparticle Interactions in Quantum Spin Chains," *Phys. Rev. Lett.* **125**, 187201 (2020).

¹⁸ V. P. Silin, "Oscillations of a Fermi-liquid in a magnetic field," *Sov. Phys. JETP* **6**, 945 (1958).

¹⁹ V. P. Silin, "The oscillations of a degenerate electron fluid," *Sov. Phys. JETP* **8**, 870 (1959).

²⁰ P. M. Platzman and P. A. Wolff, "Spin-Wave Excitation in Nonferromagnetic Metals," *Phys. Rev. Lett.* **18**, 280–283 (1967).

²¹ Sheldon Schultz and Gerald Dunifer, "Observation of Spin Waves in Sodium and Potassium," *Phys. Rev. Lett.* **18**, 283–287 (1967).

²² A. J. Leggett, "Spin diffusion and spin echoes in liquid 3 He at low temperature," *Journal of Physics C: Solid State Physics* **3**, 448 (1970).

²³ I. Dzyaloshinsky, "A thermodynamic theory of 'weak' ferromagnetism of antiferromagnetics," *J. Phys. Chem. Solids* **4**, 241 (1958).

²⁴ T. Moriya, "Anisotropic Superexchange Interaction and Weak Ferromagnetism," *Phys. Rev.* **120**, 91 (1960).

²⁵ See Supplementary Material.

²⁶ C. Giacovazzo, E. Scandale, and F. Scordari, "The crystal structure of chlorotionite, CuK₂Cl₂SO₄," *Z. Kristallogr.* **144**, 226 (1976).

²⁷ M. Hälg, W. E. A. Lorenz, K. Yu. Povarov, M. Måansson, Y. Skourski, and A. Zheludev, "Quantum spin chains with frustration due to Dzyaloshinskii-Moriya interactions," *Phys. Rev. B* **90**, 174413 (2014).

²⁸ M. Hälg, *Quantum Criticality, Universality and Scaling in Organometallic Spin-Chain Compounds* (PhD thesis, ETH Zürich, 2015).

²⁹ W. Jin and O. A. Starykh, "Phase diagram of weakly coupled Heisenberg spin chains subject to a uniform Dzyaloshinskii-Moriya interaction," *Phys. Rev. B* **95**, 214404 (2017).

³⁰ O. A. Starykh, H. Katsura, and L. Balents, "Extreme sensitivity of a frustrated quantum magnet: Cs₂CuCl₄," *Phys. Rev. B* **82**, 014421 (2010).

³¹ K. Yu. Povarov, A. I. Smirnov, O. A. Starykh, S. V. Petrov, and A. Ya. Shapiro, "Modes of Magnetic Resonance in the Spin-Liquid Phase of Cs₂CuCl₄," *Phys. Rev. Lett.* **107**, 037204 (2011).

³² S. Gangadharaiah, J. Sun, and O. A. Starykh, "Spin-orbital effects in magnetized quantum wires and spin chains," *Phys. Rev. B* **78**, 054436 (2008).

³³ Hamed Karimi and Ian Affleck, "Transverse spectral functions and Dzyaloshinskii-Moriya interactions in XXZ spin chains," *Phys. Rev. B* **84**, 174420 (2011).

³⁴ Daniel P. Arovas and Assa Auerbach, "Functional integral theories of low-dimensional quantum Heisenberg models," *Phys. Rev. B* **38**, 316–332 (1988).

³⁵ Daniel C. Dender, *Spin dynamics in the quasi-one-dimensional $S=1/2$ Heisenberg antiferromagnet copper benzoate*, Ph.D. thesis, Johns Hopkins University, Baltimore, Maryland (1997), uMI Number: 9821113.

³⁶ L. Balents and R. Egger, "Spin-dependent transport in a Luttinger liquid," *Phys. Rev. B* **64**, 035310 (2001).

³⁷ A.O. Gogolin, A.A. Nersesyan, and A.M. Tsvelik, *Bosonization and Strongly Correlated Systems* (Cambridge University Press, 2004).

³⁸ Yang-Hao Chan, Wen Jin, Hong-Chen Jiang, and Oleg A. Starykh, "Ising order in a magnetized Heisenberg chain subject to a uniform Dzyaloshinskii-Moriya interaction," *Phys. Rev. B* **96**, 214441 (2017).

³⁹ Sebastian Eggert, Ian Affleck, and Minoru Takahashi, "Susceptibility of the spin 1/2 Heisenberg antiferromag-

netic chain,” *Phys. Rev. Lett.* **73**, 332–335 (1994).

⁴⁰ Ian Affleck and Masaki Oshikawa, “Field-induced gap in Cu benzoate and other $S = \frac{1}{2}$ antiferromagnetic chains,” *Phys. Rev. B* **60**, 1038–1056 (1999).

⁴¹ Masaki Oshikawa and Ian Affleck, “Electron spin resonance in $S = \frac{1}{2}$ antiferromagnetic chains,” *Phys. Rev. B* **65**, 134410 (2002).

⁴² A. I. Smirnov, T. A. Soldatov, K. Yu. Povarov, M. Hälg, W. E. A. Lorenz, and A. Zheludev, “Electron spin resonance in a model $S = \frac{1}{2}$ chain antiferromagnet with a uniform Dzyaloshinskii-Moriya interaction,” *Phys. Rev. B* **92**, 134417 (2015).

⁴³ T. A. Soldatov, A. I. Smirnov, K. Yu. Povarov, M. Hälg, W. E. A. Lorenz, and A. Zheludev, “Spin gap in the quasi-one-dimensional $S = \frac{1}{2}$ antiferromagnet $K_2CuSO_4Cl_2$,” *Phys. Rev. B* **98**, 144440 (2018).

⁴⁴ Masanori Kohno, “Dynamically Dominant Excitations of String Solutions in the Spin-1/2 Antiferromagnetic Heisenberg Chain in a Magnetic Field,” *Phys. Rev. Lett.* **102**, 037203 (2009).

⁴⁵ Sergei Lukyanov, “Low energy effective Hamiltonian for the XXZ spin chain,” *Nuclear Physics B* **522**, 533–549 (1998).

⁴⁶ Ion Garate and Ian Affleck, “Interplay between symmetric exchange anisotropy, uniform Dzyaloshinskii-Moriya interaction, and magnetic fields in the phase diagram of quantum magnets and superconductors,” *Phys. Rev. B* **81**, 144419 (2010).

⁴⁷ Sebastian Eggert, “Numerical evidence for multiplicative logarithmic corrections from marginal operators,” *Phys. Rev. B* **54**, R9612–R9615 (1996).

⁴⁸ N. Motoyama, H. Eisaki, and S. Uchida, “Magnetic Susceptibility of Ideal Spin 1/2 Heisenberg Antiferromagnetic Chain Systems, Sr_2CuO_3 and $SrCuO_2$,” *Phys. Rev. Lett.* **76**, 3212–3215 (1996).

⁴⁹ M. Takigawa, N. Motoyama, H. Eisaki, and S. Uchida, “Dynamics in the $S = 1/2$ One-Dimensional Antiferromagnet Sr_2CuO_3 via ^{63}Cu NMR,” *Phys. Rev. Lett.* **76**, 4612–4615 (1996).

⁵⁰ M. Takigawa, O. A. Starykh, A. W. Sandvik, and R. R. P. Singh, “Nuclear relaxation in the spin-1/2 antiferromagnetic chain compound Sr_2CuO_3 : Comparison between theories and experiments,” *Phys. Rev. B* **56**, 13681–13684 (1997).

⁵¹ Victor Barzykin, “NMR relaxation rates in a spin- $\frac{1}{2}$ antiferromagnetic chain,” *Phys. Rev. B* **63**, 140412 (2001).

⁵² Z.-X. Luo, E. Lake, J.-W. Mei, and O. A. Starykh, “Spinon Magnetic Resonance of Quantum Spin Liquids,” *Phys. Rev. Lett.* **120**, 037204 (2018).

⁵³ L. Balents and O. A. Starykh, “Collective spinon spin wave in a magnetized U(1) spin liquid,” *Phys. Rev. B* **101**, 020401 (2020).

Supplemental Material for “Electron Spin Resonance of the Interacting Spinon Liquid”

Kirill Yu. Povarov,^{1,*} Timofei A. Soldatov,² Ren-Bo Wang,³
Andrey Zheludev,¹ Alexander I. Smirnov,^{2,†} and Oleg A. Starykh^{3,‡}

¹*Laboratory for Solid State Physics, ETH Zürich, 8093 Zürich, Switzerland*

²*P. L. Kapitza Institute for Physical Problems RAS, 119334 Moscow, Russia*

³*Department of Physics and Astronomy, University of Utah, Salt Lake City, Utah 84112, USA*[‡]

(Dated: August 5, 2021)

CONTENTS

I. Fermion mean-field theory of the spin-1/2 Heisenberg chain	1
A. Fermionic mapping	1
B. Mean Field description	2
C. The Larmor mode and low- q spinon continuum in applied field	3
II. The model and the unitary rotation	4
III. Low-energy model	6
A. Simplified notation	6
B. Model formulation	6
C. Connection with abelian bosonization	7
IV. $\mathbf{H} \parallel \mathbf{D}$ case	7
A. Obtaining Green’s functions	7
B. ESR Modes	8
C. ESR Intensity	10
D. Important formulas in full “experimental” notations	11
V. Renormalization group results	11
VI. Brief summary of the $\mathbf{H} \perp \mathbf{D}$ case	12
VII. Additional physical consequences of the backscattering interaction	12
VIII. Experimental information	15
A. Samples	15
B. ESR experiments	15
C. Fitting the line profiles	15
References	16

I. FERMION MEAN-FIELD THEORY OF THE SPIN-1/2 HEISENBERG CHAIN

A. Fermionic mapping

Here we sketch simple mean-field theory of the spin chain following [1] and [2, 3]. This serves to develop intuition for the more sophisticated interacting spinon description which is employed in the paper.

Start by writing spin operator on site n in terms of Abrikosov fermion $c_{n\beta}$

* povarovk@phys.ethz.ch

† smirnov@kapitza.ras.ru

‡ starykh@physics.utah.edu

$$\hat{S}_n^a = \frac{1}{2} \hat{c}_{n\alpha}^\dagger \sigma_{\alpha\beta}^a \hat{c}_{n\beta}, \quad (\text{S.1})$$

where $\alpha, \beta \in (\uparrow, \downarrow)$ are spin indices and $a = x, y, z$ denotes spin component. The convention is that repeated spin indices α, β, \dots are summed over, and therefore we do not write explicit sums over them. The fermions satisfy standard anticommutation relation $\{\hat{c}_{n\alpha}, \hat{c}_{m\beta}^\dagger\} = \delta_{n,m} \delta_{\alpha,\beta}$. This representation is exact as long as there is exactly one fermion on every site (the constraint condition)

$$\sum_{\alpha=\uparrow,\downarrow} \hat{c}_{n\alpha}^\dagger \hat{c}_{n\alpha} = 1. \quad (\text{S.2})$$

This representation converts Heisenberg Hamiltonian into that of auxiliary fermions with quartic interaction

$$\hat{\mathcal{H}} = J \sum_n \sum_{a=x,y,z} \hat{S}_n^a \hat{S}_{n+1}^a = \frac{J}{4} \sum_n \sum_{a=x,y,z} \hat{c}_{n\alpha}^\dagger \sigma^a \hat{c}_{n\beta} \hat{c}_{n+1\gamma}^\dagger \sigma^a \hat{c}_{n\delta}, \quad (\text{S.3})$$

but Fierz identity

$$\sum_a \sigma_{\alpha\beta}^a \sigma_{\gamma\delta}^a = 2\delta_{\alpha\delta} \delta_{\beta\gamma} - \delta_{\alpha\beta} \delta_{\gamma\delta} \quad (\text{S.4})$$

helps to simplify it. Namely,

$$\hat{\mathcal{H}} = \frac{J}{4} \sum_n \left(2\hat{c}_{n\alpha}^\dagger \hat{c}_{n\beta} \hat{c}_{n+1\beta}^\dagger \hat{c}_{n+1\alpha} - \hat{c}_{n\alpha}^\dagger \hat{c}_{n\alpha} \hat{c}_{n\gamma}^\dagger \hat{c}_{n\gamma} \right). \quad (\text{S.5})$$

Notice that the last term in the above equation is, according to the constraint (S.2), the product of identity operators and contributes trivial constant to H , which we omit in the following. Therefore the Hamiltonian

$$\hat{\mathcal{H}} = -\frac{J}{2} \sum_n \hat{c}_{n\alpha}^\dagger \hat{c}_{n+1\alpha} \hat{c}_{n+1\beta}^\dagger \hat{c}_{n\beta} \quad (\text{S.6})$$

is now written in terms of the bond operator $\hat{\mathcal{B}}_{n,n+1} = \hat{c}_{n\alpha}^\dagger \hat{c}_{n+1\alpha} = \hat{c}_{n\uparrow}^\dagger \hat{c}_{n+1\uparrow} + \hat{c}_{n\downarrow}^\dagger \hat{c}_{n+1\downarrow}$ and its conjugate $\hat{\mathcal{B}}_{n,n+1}^\dagger = \hat{\mathcal{B}}_{n+1,n}$.

B. Mean Field description

Up to now the manipulations are exact. Now we proceed with the mean field approximation by introducing position-independent and real vacuum expectation value [1]

$$\mathcal{D} = \langle \hat{c}_{n\uparrow}^\dagger \hat{c}_{n+1\uparrow} + \hat{c}_{n\downarrow}^\dagger \hat{c}_{n+1\downarrow} \rangle \neq 0 \quad (\text{S.7})$$

and assuming that fluctuations of $\hat{\mathcal{B}}_{n,n+1}$ about \mathcal{D} are *small*. This assumption, consistency of which is checked a posteriori [1], allows us to neglect quadratic in this smallness terms $(\hat{\mathcal{B}}_{n,n+1} - \mathcal{D})(\hat{\mathcal{B}}_{n+1,n} - \mathcal{D}) \rightarrow 0$ and obtain

$$\begin{aligned} \hat{\mathcal{H}} &= -\frac{J}{2} \sum_n (\mathcal{D} + \hat{\mathcal{B}}_{n,n+1} - \mathcal{D})(\mathcal{D} + \hat{\mathcal{B}}_{n+1,n} - \mathcal{D}) \approx -\frac{J}{2} \sum_n \mathcal{D}^2 + \mathcal{D}(\hat{\mathcal{B}}_{n,n+1} - \mathcal{D} + \hat{\mathcal{B}}_{n+1,n} - \mathcal{D}) \\ &= \frac{J}{2} \sum_n \mathcal{D}^2 - \frac{J}{2} \sum_n \mathcal{D}(\hat{\mathcal{B}}_{n,n+1} + \hat{\mathcal{B}}_{n+1,n}) \rightarrow -\frac{J\mathcal{D}}{2} \sum_n (\hat{c}_{n\alpha}^\dagger \hat{c}_{n+1\alpha} + \hat{c}_{n+1\alpha}^\dagger \hat{c}_{n\alpha}), \end{aligned} \quad (\text{S.8})$$

where in the last step we dropped unessential constant $\propto \mathcal{D}^2$ from the previous one.

The last expression in (S.8) describes non-interacting fermions. It is now straightforward to Fourier transform to the k -space

$$\hat{c}_{n\alpha} = \frac{1}{\sqrt{N}} \sum_k e^{-ikn} \hat{c}_{k\alpha} \quad (\text{S.9})$$

and also to add magnetic field via the Zeeman interaction term

$$-\sum_n g\mu_B H \hat{S}_n^z = -\frac{1}{2} g\mu_B H \sum_n (\hat{c}_{n\uparrow}^\dagger \hat{c}_{n\uparrow} - \hat{c}_{n\downarrow}^\dagger \hat{c}_{n\downarrow}) = -\frac{1}{2} g\mu_B H \sum_k (\hat{c}_{k\uparrow}^\dagger \hat{c}_{k\uparrow} - \hat{c}_{k\downarrow}^\dagger \hat{c}_{k\downarrow}). \quad (\text{S.10})$$

In this way we arrive at the Mean Field Hamiltonian of the spin chain in the magnetic field (here \uparrow corresponds to $\alpha = +1$ and \downarrow to $\alpha = -1$)

$$\hat{\mathcal{H}}_{\text{MF}} = \sum_k \sum_{\alpha=\pm 1} \left(-J\mathcal{D} \cos(k) - \frac{1}{2} g\mu_B H \alpha \right) \hat{c}_{k\alpha}^\dagger \hat{c}_{k\alpha} \quad (\text{S.11})$$

C. The Larmor mode and low- q spinon continuum in applied field

Without the magnetic field the fermion band is half-filled (due to the constraint (S.2)) which means that its Fermi wavevector is $k_F = \pi/(2a)$. Finite magnetic field splits this degeneracy, resulting in different Fermi wavevectors for \uparrow - and \downarrow -spin fermions,

$$\langle \hat{S}^z \rangle = \frac{1}{2}(n_\uparrow - n_\downarrow) = \frac{1}{2} \int_{-\pi}^{\pi} \frac{dka}{2\pi} (n_\uparrow(k) - n_\downarrow(k)) = \frac{a}{2\pi} (k_{F\uparrow} - k_{F\downarrow}) \quad (\text{S.12})$$

where $\langle \hat{S}^z \rangle$ is the average spin angular momentum per site of the chain. Note that this implies that the spin angular momentum density M is given by $\langle \hat{S}^z \rangle/a$. The number of \uparrow -fermions grows, $k_{F\uparrow} \rightarrow k_{F\uparrow} + \Delta k_F$, while that of \downarrow -fermions decreases, $k_{F\downarrow} \rightarrow k_{F\downarrow} - \Delta k_F$. Therefore

$$\Delta k_F = \pi M \quad (\text{S.13})$$

changes from 0 for the non-magnetized chain to the maximum possible value of $\pi/(2a)$ for the fully magnetized one ($\langle \hat{S}^z \rangle = 1/2$), when the \downarrow -fermion band is completely depopulated.

The above picture provides a very intuitive way of understanding the structure of low- q continuum depicted in Fig. 2a of the main text. Naturally, the susceptibilities χ^\pm and χ^\mp correspond to spin-flip transitions \downarrow, \uparrow -to- \uparrow, \downarrow in the neighborhood of the zero-field Fermi momentum $\pi/2a$, and vice versa. A very special transition, with the zero momentum change $q = 0$ and the energy transfer of $g\mu_B H$, is the Larmor resonance. Since $g\mu_B H$ is exactly the Zeeman energy splitting of the Fermi surface, many electrons (4 Δk_F of them) contribute to it, as Fig. 1(left) shows. This is true for both linear and non-linear spinon dispersions, e.g. such as a cosine one in (S.11). Generally, this is not the case for $q \neq 0$ transitions and the non-linear dispersion of spinons, Fig. 1(left).

Details of the non-interacting spinon continuum in Figs. 1 and 2 are understood from the transverse susceptibility

$$\chi^\pm(x, t) = -i\Theta(t) \langle [S^+(x, t), S^-(0, 0)] \rangle = -i\Theta(t) \frac{1}{N^2} \sum_{k, k'} \sum_{k_1, k_2} e^{i\epsilon_k - \epsilon_{k'} - g\mu_B H)t} e^{-i(k-k')x} \langle [\hat{c}_{k\uparrow}^\dagger \hat{c}_{k'\downarrow}, \hat{c}_{k_1\downarrow}^\dagger \hat{c}_{k_2\uparrow}] \rangle, \quad (\text{S.14})$$

where we parameterized spin- α spinon dispersion as $\epsilon_k - \frac{1}{2} g\mu_B H \alpha$. Eq.(S.11) corresponds to $\epsilon_k = -J \cos(k)$ (we absorb \mathcal{D} into J for simplicity). Other dispersion relations are possible as well, and results for the linear and parabolic ones are presented in Fig. 2. The commutator in (S.14) is easily evaluated to be

$$\langle [\hat{c}_{k\uparrow}^\dagger \hat{c}_{k'\downarrow}, \hat{c}_{k_1\downarrow}^\dagger \hat{c}_{k_2\uparrow}] \rangle = \delta_{k', k_1} \delta_{k, k_2} \left(f(\epsilon_k - g\mu_B H/2) - f(\epsilon_{k'} + g\mu_B H/2) \right), \quad (\text{S.15})$$

where f is the Fermi function $f(x) = 1/(e^{x/T} + 1) \rightarrow \Theta(-x)$ in the zero-temperature limit $T \rightarrow 0$. Fourier transforming

$$\chi^\pm(q, \omega) = \int dt \int dx e^{-iqx+i\omega t} \chi^\pm(x, t) = \frac{1}{N} \sum_k \frac{f(\epsilon_k - g\mu_B H/2) - f(\epsilon_{k'} + g\mu_B H/2)}{\omega - g\mu_B H + \epsilon_k - \epsilon_{k+q} + i0} \quad (\text{S.16})$$

so that the imaginary part is

$$\text{Im}(\chi^\pm(q, \omega)) = -\pi \int \frac{dk}{2\pi} (\Theta(-\epsilon_k + g\mu_B H/2) - \Theta(-\epsilon_{k+q} - g\mu_B H/2)) \delta(\omega - g\mu_B H + \epsilon_k - \epsilon_{k+q}). \quad (\text{S.17})$$

Step-functions select two integration intervals: $(\pi/2 - \phi - q, \pi/2 + \phi)$ and $(-\pi/2 - \phi, -\pi/2 + \phi - q)$ where $\sin \phi = g\mu_B H/(2J)$. The first of these corresponds to the right-moving fermions while the second - to the left ones. Focusing on the right movers, set $k = \pi/2 + p - q/2$ so that the argument of the delta-function becomes $\omega - g\mu_B H - 2J \sin(q/2) \cos(p)$. The p -integration is simple and leads to the right-movers contribution to χ

$$\text{Im}(\chi_R^\pm(q, \omega)) = \frac{-1}{\sqrt{(2J \sin q/2)^2 - (\omega - g\mu_B H)^2}} \text{ where } 2J \sin(q/2) \cos(\phi + q/2) \leq \omega - g\mu_B H \leq 2J \sin(q/2) \quad (\text{S.18})$$

This is seen as the upward branch in Fig.1(right) emerging from $g\mu_B H$. Contribution of the left-moving fermions has identical functional form but the frequency is bounded by $2J \sin(q/2) \cos(\phi - q/2) \leq \omega - g\mu_B H \leq 2J \sin(q/2)$. This is seen to be extremely narrow, essentially a single line, downward branch in Fig.1(right). $\text{Im}(\chi^\mp(q, \omega))$ is obtained from (S.18) by $H \rightarrow -H$.

Figure 2 shows examples of the spinon continua for different ϵ_k . In particular, for the linear dispersion (which is the case of our Hamiltonian (2) in the main text) susceptibility (S.17) reduces to the sum of $\delta(\omega - g\mu_B H \pm v_F k)$ as described in the main text. Interactions (different from the backscattering one we consider in this work) do spread spinon continuum outside the narrow intervals obtained in (S.18) and below [4]. But most of the spectral weight remains to be sharply focused on the boundaries of the non-interacting spinon continuum, in a delta-function-like fashion.

Backscattering interaction u changes this picture qualitatively, by shifting the spinon continuum up in energy and producing a spin-1 oscillatory collective mode of spinons [5], that originates from the Larmor frequency at $q = 0$. Its effect on the spin chain with the uniform DM interaction is described in the main text, while key technical steps are summarized below.

II. THE MODEL AND THE UNITARY ROTATION

Consider a one-dimensional (1D) antiferromagnetic XXZ spin- $\frac{1}{2}$ Heisenberg chain with a uniform Dzyaloshinskii-Moriya (DM) interaction $\mathbf{D} = (0, 0, D)$ in the presence of an external magnetic field $\mathbf{H} = (0, 0, H)$ [4, 6–8]

$$\hat{\mathcal{H}} = J \sum_j (\hat{S}_j^x \hat{S}_{j+1}^x + \hat{S}_j^y \hat{S}_{j+1}^y + \hat{S}_j^z \hat{S}_{j+1}^z) - D \sum_j (\hat{S}_j^x \hat{S}_{j+1}^y - \hat{S}_j^y \hat{S}_{j+1}^x) - \sum_j g\mu_B H \hat{S}_j^z. \quad (\text{S.19})$$

Since $\mathbf{H} \parallel \mathbf{D}$, an important general consideration is possible on the level of the lattice Hamiltonian. Namely, we rotate spins about z -axis as

$$\hat{S}_n^+ = \hat{\tilde{S}}_n^+ e^{iq_{\text{DM}} n a}, \hat{S}_n^z = \hat{\tilde{S}}_n^z \quad (\text{S.20})$$

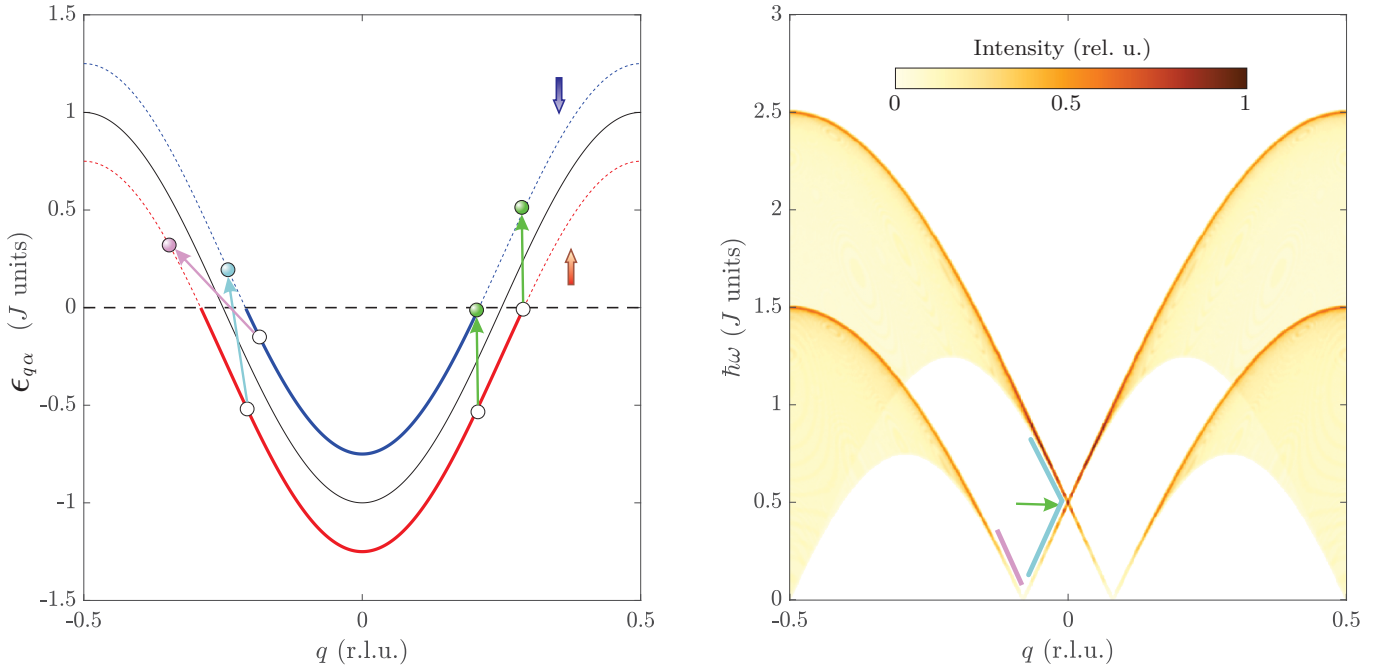
where

$$q_{\text{DM}} = \tan^{-1}(D/J)/a \approx \frac{D}{Ja} \quad (\text{S.21})$$

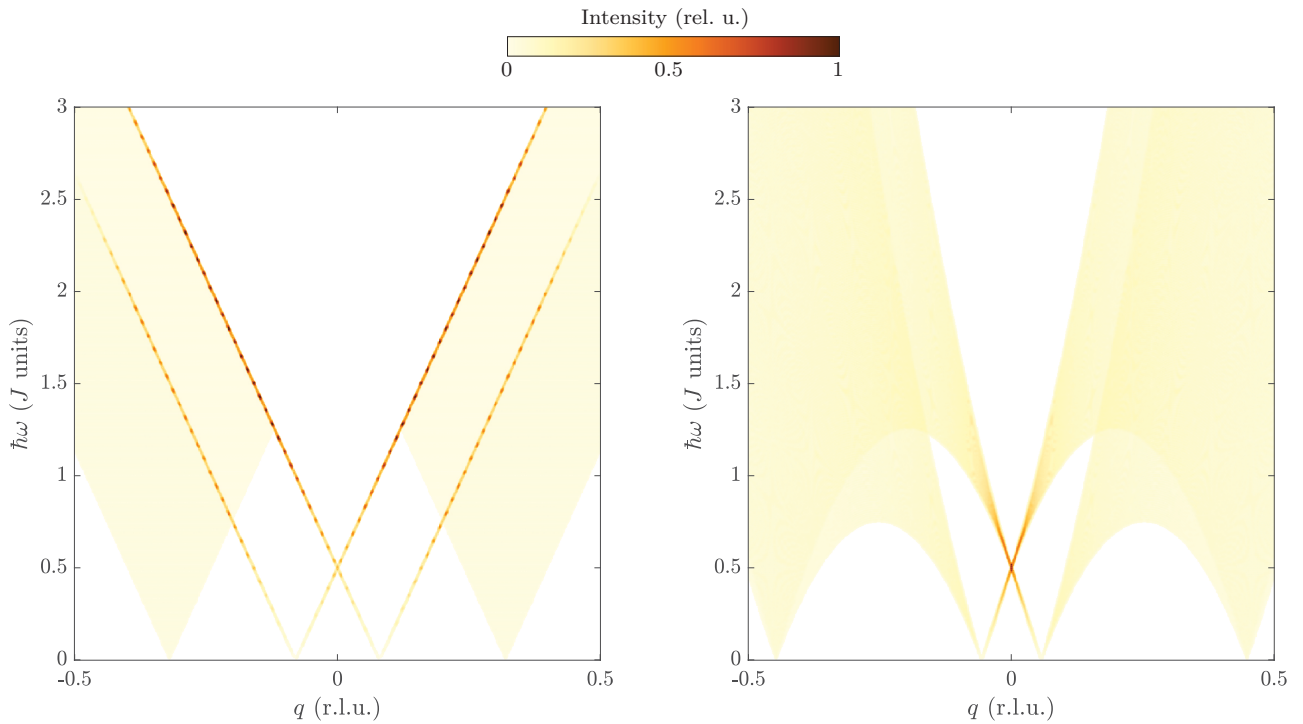
and $x = na$ is the coordinate of the n -th spin along the chain.

The Hamiltonian (S.19) transforms into

$$\hat{\mathcal{H}} = \sqrt{J^2 + D^2} \sum_n [\frac{1}{2} (\hat{\tilde{S}}_n^+ \hat{\tilde{S}}_{n+1}^- + \hat{\tilde{S}}_n^- \hat{\tilde{S}}_{n+1}^+) + \frac{J}{\sqrt{J^2 + D^2}} \hat{\tilde{S}}_n^z \hat{\tilde{S}}_{n+1}^z] - g\mu_B H \sum_n \hat{\tilde{S}}_n^z. \quad (\text{S.22})$$



SUPP. FIG. 1. Left: spinon dispersions for up and down values of spin α in the applied field $g\mu_B H = 0.5J$. The typical spin-flip transitions scenarios with small momentum transfer q are shown. Right: the resulting transverse two-spinon continuum. Sections of the spectra originating from the transitions illustrated by colored arrows in the left panel are highlighted by the same colors in the right panel.



SUPP. FIG. 2. Two-fermion spin-flip continuum for the toy models with linear dispersion $\epsilon_q = J(q - 1)$ (left) and parabolic dispersion $\epsilon_q = J(\frac{q^2}{2J} - 1)$ (right). Zeeman energy is $g\mu_B H = 0.5J$ in both cases.

Here we see that (S.22) is just a chain without the DM interaction with exchange interaction $\tilde{J} = \sqrt{J^2 + D^2} \approx J + D^2/(2J)$ and anisotropy parameter $\tilde{\Delta} = \frac{J}{\sqrt{J^2 + D^2}} \approx 1 - D^2/(2J^2)$. For the chain with $D \ll J$, which is the case of our interest, these quadratic deviations can be neglected.

The most important consequence of the simple transformation (S.20) is that the dynamic structure factor $\mathcal{S}(q, \omega)$ of the Hamiltonian (S.19) is given by the dynamic structure factor $\tilde{\mathcal{S}}(q + q_{\text{DM}}, \omega)$ of the rotated Hamiltonian (S.22) but with the boosted momentum $q + q_{\text{DM}}$. In particular, the ESR response of the original model, which is proportional to $\mathcal{S}(0, \omega)$ is seen to be given by that of the essentially ideal spin chain (up to omitted D^2/J^2 terms) $\tilde{\mathcal{S}}(q_{\text{DM}}, \omega)$ but at the finite momentum $q_{\text{DM}} = D/(Ja)$.

This crucial feature turns the standard ESR probe into the finite momentum one and allows us to explore details of the small-momentum response of the spin-1/2 chain in the magnetic field with accuracy greatly exceeding that of the inelastic neutron scattering experiments.

III. LOW-ENERGY MODEL

A. Simplified notation

In the following part we are going to use the simplified notation. The following correspondences are used:

- Zeeman energy as the magnetic field equivalent $g\mu_B H \rightarrow B$
- Excitation energy $h\nu \rightarrow \omega$
- Susceptibility per unit of chain length $\chi_0 = \frac{(g\mu_B)^2}{2\pi v} = \frac{(g\mu_B)^2}{a\pi^2 J}$ is expressed as $1/\pi^2 J$ (corresponding to *single spin* susceptibility with respect to field B defined above)

Effectively, in this simplified notation the lattice constant a , $g\mu_B$, and \hbar are all set to 1.

B. Model formulation

The spin operators are approximated as [6, 8, 9]

$$\hat{\mathbf{S}}_n \rightarrow [\hat{\mathbf{J}}_L(x) + \hat{\mathbf{J}}_R(x) + (-1)^x \hat{\mathbf{N}}(x)], \quad (\text{S.23})$$

$x = n$ is the spin position, $\hat{\mathbf{J}}_L$ and $\hat{\mathbf{J}}_R$ are the uniform components of the left/right spin-currents, respectively, and $\hat{\mathbf{N}}$ is the staggered component of the local spin density. The low-energy effective Hamiltonian can be written in the Sugawara form,

$$\hat{\mathcal{H}} = \hat{\mathcal{H}}_0 + \hat{V}_{\text{bs}} + \hat{\mathcal{H}}', \quad (\text{S.24})$$

$$\hat{\mathcal{H}}_0 = \frac{2\pi}{3} v_F \int dx : \hat{\mathbf{J}}_R \cdot \hat{\mathbf{J}}_R + \hat{\mathbf{J}}_L \cdot \hat{\mathbf{J}}_L : , \quad (\text{S.25})$$

$$\hat{V}_{\text{bs}} = -u \int dx : \hat{\mathbf{J}}_R \cdot \hat{\mathbf{J}}_L + \lambda \hat{J}_R^z \hat{J}_L^z : , \quad (\text{S.26})$$

$$\hat{\mathcal{H}}' = -B \int dx (\hat{J}_R^z + \hat{J}_L^z) - \tilde{D} \int dx (\hat{J}_R^z - \hat{J}_L^z), \quad (\text{S.27})$$

where $v_F = \pi J/2$ is the speed of the low-energy excitations, columns $: :$ denote normal ordering, and $\lambda \sim D^2/J^2 \ll 1$ is the effective anisotropy parameter (which we neglect in the following), and $\tilde{D} \sim D$ is the DM interaction. The backscattering interaction is denoted by u . It plays the key role in our study.

It is remarkable fact [9] that (S.24) can be re-written in terms of spin-1/2 Dirac fermions $\psi_{R,s}, \psi_{L,s}$ subject to backscattering interaction $\hat{V}_{\text{bs}} = -u \int dx \hat{\mathbf{J}}_R \cdot \hat{\mathbf{J}}_L$. Here the right spin current $\hat{\mathbf{J}}_R = \frac{1}{2} \hat{\psi}_R^\dagger \boldsymbol{\sigma} \hat{\psi}_R$ and similarly for the left current. The notation is that $\hat{\psi}_R$ without spin subindex s denotes two-component spinor $\hat{\psi}_R = (\hat{\psi}_{R\uparrow}, \hat{\psi}_{R\downarrow})^T$. The full Hamiltonian is $\hat{\mathcal{H}} = \hat{\mathcal{H}}_0 + \hat{\mathcal{H}}' + \hat{V}_{\text{bs}}$ where the free part $\hat{\mathcal{H}}_0$ describes fermion kinetic energy and $\hat{\mathcal{H}}'$ collects DM and Zeeman interactions

$$\hat{\mathcal{H}}_0 + \hat{\mathcal{H}}' = \int \left[v_F \left(\hat{\psi}_R^\dagger (-i\partial_x) \hat{\psi}_R + \hat{\psi}_L^\dagger (i\partial_x) \hat{\psi}_L \right) - B(\hat{J}_R^z + \hat{J}_L^z) - \tilde{D}(\hat{J}_R^z - \hat{J}_L^z) \right] dx \quad (\text{S.28})$$

Note that the magnetization operator $\hat{M} = \hat{J}_R^z + \hat{J}_L^z$ is just the sum of the right and left spin currents. Its expectation value is magnetization itself, $M = \langle \hat{J}_R^z + \hat{J}_L^z \rangle$.

The backscattering interaction is broken into transverse and longitudinal parts, $\hat{V}_{\text{bs}} = \hat{V}_1 + \hat{V}_2$, where

$$\hat{V}_1 = -\frac{u}{2} \int dx \left(\hat{J}_R^+ \hat{J}_L^- + \hat{J}_R^- \hat{J}_L^+ \right) = -\frac{u}{2} \int dx \left(\hat{\psi}_{R\uparrow}^\dagger \hat{\psi}_{R\downarrow} \hat{\psi}_{L\downarrow}^\dagger \hat{\psi}_{L\uparrow} + \hat{\psi}_{R\downarrow}^\dagger \hat{\psi}_{R\uparrow} \hat{\psi}_{L\uparrow}^\dagger \hat{\psi}_{L\downarrow} \right) \quad (\text{S.29})$$

and

$$\hat{V}_2 = -u \int dx \hat{J}_R^z \hat{J}_L^z = -\frac{u}{4} \int dx (\hat{\psi}_{R\uparrow}^\dagger \hat{\psi}_{R\uparrow} - \hat{\psi}_{R\downarrow}^\dagger \hat{\psi}_{R\downarrow}) (\hat{\psi}_{L\uparrow}^\dagger \hat{\psi}_{L\uparrow} - \hat{\psi}_{L\downarrow}^\dagger \hat{\psi}_{L\downarrow}). \quad (\text{S.30})$$

C. Connection with abelian bosonization

For completeness, here we write down abelian form of equations (S.28), (S.29) and (S.30). Chapter 18 of Ref. [9], see also Appendix A in [8], shows that

$$\hat{\mathcal{H}}_0 + \hat{V}_2 = \int dx \frac{1}{2} [v_F K_s (\partial_x \theta_s)^2 + \frac{v_F}{K_s} (\partial_x \varphi_s)^2], \quad K_s = 1 + \frac{u}{4\pi v_F} \quad (\text{S.31})$$

$$\hat{\mathcal{H}}' = - \int dx \left(\frac{B}{\sqrt{2\pi}} \partial_x \varphi_s - \frac{\tilde{D}}{\sqrt{2\pi}} \partial_x \theta_s \right) \quad (\text{S.32})$$

$$\hat{V}_1 = -\frac{u}{4\pi^2} \int dx \cos \sqrt{8\pi} \varphi_s \quad (\text{S.33})$$

Observe that longitudinal part of the backscattering interaction, term \hat{V}_2 , adds to the non-interacting Hamiltonian $\hat{\mathcal{H}}_0$. This apparent simplicity, however, hides spin-rotational invariance of the theory. In the $u \rightarrow 0$ limit, which takes place at $T = 0$ and for $B = 0$, the Hamiltonian reduces to the non-interacting one, with $K_s = 1$ and $\hat{V}_1 = 0$. For the purpose of our study, the fermion formulation of the theory in Section III B is much more convenient.

IV. $\mathbf{H} \parallel \mathbf{D}$ CASE

A. Obtaining Green's functions

In the low-energy regime, we use the path integral formulation of the partition function which we supplement with the action of the auxiliary vector fields $\lambda_r(x, \tau)$

$$Z[\lambda_R, \lambda_L] = \int [\mathcal{D}\bar{\psi}_{R/L} \mathcal{D}\psi_{R/L}] e^{S_0 + S_{\text{int}}} \int [\mathcal{D}\lambda_R] [\mathcal{D}\lambda_L] e^{-\frac{1}{u} \int_0^\beta d\tau \int dx \lambda_R^T(x, \tau) \cdot \lambda_L(x, \tau)}, \quad (\text{S.34})$$

where $\psi_{sr}, \bar{\psi}_{sr}$ are the fermion fields with spin $s = \uparrow, \downarrow$ and chirality $r = R, L$, and S_0, S_{int} are noninteracting and interacting parts of the action, respectively. The free action is determined by $\hat{\mathcal{H}}_0 + \hat{\mathcal{H}}'$. The interaction action is determined by the backscattering Hamiltonian, $S_{\text{int}} = - \int d\tau \hat{V}_{\text{bs}}$. We next shift fields $\lambda_r(x, \tau)$ by the corresponding current, as $\lambda_r(x, \tau) \rightarrow \lambda_r(x, \tau) + u \mathbf{J}_r(x, \tau)$, which removes S_{int} term altogether, thereby achieving a Hubbard-Stratonovich transformation. The resultant action is quadratic in fermions ψ_{sr} but now contains $\lambda_r(x, \tau) \cdot \mathbf{J}_r(x, \tau)$ terms. We next integrate fermions out, evaluate effective action of λ_r fields to second order (the loop expansion) and then integrate them out as well. The end result of this procedure is the exponential written in terms of the quadratic from of the source fields (introduced earlier in the process). The coefficients of this form are given by the Matsubara Green's functions of the spin currents.

The longitudinal and transverse retarded susceptibilities can be obtained via analytical continuation from the Matsubara Green's functions

$$G^{zz}(q, \nu_n) = - \int_{-\infty}^{\infty} dx e^{-iqx} \int d\tau e^{i\nu_n \tau} \langle T_{\tau} \hat{J}^z(x, \tau) \hat{J}^z(0) \rangle, \quad (\text{S.35})$$

$$G^{+-}(q, \nu_n) = - \int_{-\infty}^{\infty} dx e^{-iqx} \int d\tau e^{i\nu_n \tau} \langle T_{\tau} \hat{J}^+(x, \tau) \hat{J}^-(0) \rangle. \quad (\text{S.36})$$

To the 2nd order in the loop expansion,

$$\begin{aligned} \chi_R^{zz}(q, \omega) &= G^{zz}(q, i\nu_n \rightarrow \omega + i0) \\ &= \frac{1}{2} \chi_- \tilde{v} q \left(\frac{1}{\hbar\omega - \hbar\tilde{v}q + i0} - \frac{1}{\omega + \tilde{v}q + i0} \right), \\ \chi_R^{+-}(q, \omega, M_+, M_-) &= G^{+-}(q, i\nu_n \rightarrow \omega + i0, M_+, M_-) \\ &= \frac{A_+(q, M_+, M_-)}{\omega - \omega_+(q, M_+, M_-) + i0} + \frac{A_-(q, M_+, M_-)}{\omega - \omega_-(q, M_+, M_-) + i0} \\ &= \chi_R^{-+}(-q, \omega, -M_+, M_-), \end{aligned} \quad (\text{S.37})$$

where $\chi_{\pm} = \chi_0 / (1 \pm \frac{1}{2}u\chi_0)$, $\tilde{v} = v_F \sqrt{1 - (\frac{1}{2}u\chi_0)^2}$ and

$$M_{\pm} = M_R \pm M_L = \chi_{\mp} \begin{cases} B \\ \tilde{D} \end{cases}, \quad (\text{S.38})$$

are the magnetization and the spin current. The energies of the collective spin-1 modes are

$$\hbar\omega_{\pm}(q, M_+, M_-) = \frac{M_+}{\chi_0} \pm \sqrt{\left(\frac{1}{2}uM_+\right)^2 + [\tilde{v}(q + 2\pi M_-)]^2} \quad (\text{S.39})$$

$$= -\hbar\omega_{\mp}(q, -M_+, M_-), \quad (\text{S.40})$$

while their spectral weights (residues) are

$$A_{\pm}(q, M_+, M_-) = M_+ \pm \frac{-\frac{1}{2}uM_+^2 + \chi_-[\tilde{v}(q + 2\pi M_-)]^2}{\sqrt{\left(\frac{1}{2}uM_+\right)^2 + [\tilde{v}(q + 2\pi M_-)]^2}}, \quad (\text{S.41})$$

$$= -A_{\mp}(q, -M_+, M_-). \quad (\text{S.42})$$

Eq. (S.38) constitutes the Onsager relation for our problem, it provides access to χ^{-+} without additional calculations.

B. ESR Modes

At this point it is useful to recall that $\chi_0 = 1/(2\pi v_F)$ and to introduce the dimensionless interaction parameter δ as

$$\delta = \frac{1}{2}u\chi_0 = \frac{u}{4\pi v_F}. \quad (\text{S.43})$$

Then

$$\omega_{\pm}(q, B, \tilde{D}) = B + \frac{\delta}{1 - \delta} B \pm \sqrt{\left(\frac{\delta}{1 - \delta} B\right)^2 + \left[\tilde{v}\left(q + \frac{\tilde{D}}{v_F(1 + \delta)}\right)\right]^2} \quad (\text{S.44})$$

From here we can identify the momentum boost q_{DM} in (S.20) with $\tilde{D}/(v_F(1 + \delta))$ which leads to

$$\tilde{D} = (1 + \delta) \frac{v_F}{J} D \approx \frac{\pi}{2} (1 + \delta) D. \quad (\text{S.45})$$

This establishes the relation between the DM parameter of the lattice Hamiltonian (S.19) and the parameter \tilde{D} of the continuum low-energy theory (S.27).

Thus, at $q = 0$ we have

$$\omega_{\pm}(0, B, D) = B + \frac{\delta}{1 - \delta} B \pm \sqrt{\left(\frac{\delta}{1 - \delta} B\right)^2 + (1 - \delta^2) \left(\frac{\pi}{2} D\right)^2}. \quad (\text{S.46})$$

For practical purposes, the coefficient of the last term under the square root can be approximated $1 - \delta^2 \approx 1$ due to exceedingly small correction represented by $(\delta D)^2$ term. Observe that

$$\Delta\omega \equiv \omega_+ - \omega_- = 2 \sqrt{\left(\frac{\delta}{1 - \delta} B\right)^2 + \left(\frac{\pi}{2} D\right)^2}, \quad (\text{S.47})$$

which suggests the plot of $(\Delta\omega/2)^2$ versus B^2 should be a straight line with the slope $(\delta/(1 - \delta))^2$ and the vertical axis intercept $(\pi D/2)^2$.

The residues at $q = 0$ also simplify,

$$A_{\pm}(0, B, D) = \chi_- \left\{ B \pm \frac{(\pi D/2)^2 - B^2 \delta/(1 - \delta)}{\sqrt{\left(\frac{\delta}{1 - \delta} B\right)^2 + \left(\frac{\pi}{2} D\right)^2}} \right\} \quad (\text{S.48})$$

Note that within the linear response theory the absorption intensity per unit length is given by

$$I(\omega) = -\frac{1}{2} H_{\text{rad}}^2 \omega \text{Im}[\chi_R(0, \omega, B, D)] \quad (\text{S.49})$$

where H_{rad} is the amplitude of the radiation (microwave) field. In our case from (S.38) we obtain

$$\text{Im}[\chi_R(0, \omega, B, D)] = -\pi \left(A_+ \delta(\omega - \omega_+) + A_- \delta(\omega - \omega_-) \right). \quad (\text{S.50})$$

Observe that $\omega_+ > 0$ for all fields and therefore contributes to the ESR signal for all fields $B \in (0, \infty)$. The lower branch, ω_- , becomes positive for $B > B_1$, see (S.55) below. Thus for that branch $B \in (B_1, \infty)$.

The total intensity of this polarization is therefore the sum of the two contributions

$$I^{+-}(\omega) = \frac{\pi}{2} H_{\text{rad}}^2 (\omega_+ A_+ \delta(\omega - \omega_+) + \omega_- A_- \delta(\omega - \omega_-)). \quad (\text{S.51})$$

Correspondingly, the ratio of the intensities of the upper and lower ESR branches is given by

$$\frac{I_+^{+-}}{I_-^{+-}} = \left(\frac{\omega_+}{\omega_-}\right) \left(\frac{A_+}{A_-}\right) \quad (\text{S.52})$$

Next we turn to χ^{-+} , the opposite circular polarization. Using (S.38), (S.40) and (S.42), we find that χ^{-+} is written in terms (S.44) and (S.48) as

$$\chi_R^{-+}(0, \omega, B, D) = \frac{-A_-(0, B, D)}{\omega + \omega_-(0, B, D) + i0} + \frac{-A_+(0, B, D)}{\omega + \omega_+(0, B, D) + i0} \quad (\text{S.53})$$

Since $\omega_+(0, B, D) > 0$ for all B, D , the 2nd term in the above does not contribute to the imaginary part. We find

$$\begin{aligned} \text{Im}[\chi_R^{-+}(0, \omega, B, D)] &= -\pi(-A_-(0, B, D))\delta(\omega + \omega_-(0, B, D)) \\ &= -\pi\chi_- \left\{ \frac{(\pi D/2)^2 - \delta/(1-\delta)B^2}{\sqrt{\left(\frac{\delta}{1-\delta}B\right)^2 + \left(\frac{\pi}{2}D\right)^2}} - B \right\} \delta\left(\omega + \frac{B}{1-\delta} - \sqrt{\left(\frac{\delta B}{1-\delta}\right)^2 + \left(\frac{\pi}{2}D\right)^2}\right) \end{aligned} \quad (\text{S.54})$$

This branch contributes in only the narrow field interval $B \in (0, B_1)$ where

$$B_1 = \sqrt{\frac{1-\delta}{1+\delta} \frac{\pi D}{2}} \quad (\text{S.55})$$

is the maximum field for the response in this polarization since $\omega_-(0, B_1, D) = 0$. It is also easy to check that $-A_-(0, B_1, D) = 0$. The intensity of this branch also follows from (S.49),

$$I^{-+}(\omega) = \frac{\pi}{2} H_{\text{rad}}^2 \omega_-(0, B, D) (-A_-(0, B, D)) \delta(\omega + \omega_-). \quad (\text{S.56})$$

C. ESR Intensity

Eq.(S.66) describes ratio of intensities at a given (fixed) magnetic field, when frequencies of the two modes are different. But the experiment is done at fixed resonator frequency by adjusting external magnetic field, i.e. the two branches contribute at the same frequency which occurs at different resonance fields for them. To account for this, we need to switch from sum of delta-functions $\delta(\omega - \omega_{\pm})$ to the one which depends on magnetic field B , $\delta(B - B_{\pm})$.

Thus let (set $d = \pi D/2$ for a moment)

$$\omega = \frac{B_{\pm}}{1-\delta} \pm \sqrt{\left(\frac{\delta B_{\pm}}{1-\delta}\right)^2 + (1-\delta^2)d^2}. \quad (\text{S.57})$$

We find

$$B_{\pm} = \frac{\omega \mp S}{1+\delta}, \quad S = \sqrt{\delta^2\omega^2 + (1-\delta^2)^2d^2}. \quad (\text{S.58})$$

By construction, $\omega_+(B_+) = \omega = \omega_-(B_-)$ and $B_- - B_+ = 2S/(1+\delta) > 0$. Next, we need to “solve” the delta function $\delta(\omega - \omega_{\pm})$ by using $\omega_{\pm}(H) = \omega_{\pm}(B_{\pm}) + (B - B_{\pm})\omega'_{\pm}$, where $\omega'_{\pm} \equiv (d\omega_{\pm}(B)/dB)|_{B=B_{\pm}}$. Then $\delta(\omega - \omega_{\pm}) = \delta(B - B_{\pm})/|\omega'_{\pm}|$. Using this result and after considerable algebra we find that (S.51) is replaced by

$$I_{\omega}^{+-}(H) = \frac{1}{2} H_{\text{rad}}^2 \omega \frac{\pi \chi_0}{1-\delta} \left(\frac{S + \delta\omega}{S} \delta(B - B_-) + \frac{S - \delta\omega}{S} \delta(B - B_+) \right). \quad (\text{S.59})$$

Therefore we get for the ratio of the intensities at the same frequency

$$\mathcal{R} = \frac{I_{\omega}^{+-}(B_+)}{I_{\omega}^{+-}(B_-)} = \frac{\sqrt{(\delta\omega)^2 + (1-\delta^2)^2(\pi D/2)^2} - \delta\omega}{\sqrt{(\delta\omega)^2 + (1-\delta^2)^2(\pi D/2)^2} + \delta\omega}. \quad (\text{S.60})$$

This simple result has few nice features. For non-interacting spinons ($\delta = 0$) we obtain $\mathcal{R} = 1$, while for the interacting ones but with no DM interaction ($D = 0$) we have $\mathcal{R} = 0$ (since in this case one is probing at strictly $q = 0$). For both $\delta \neq 0$ and $D \neq 0$ we see that \mathcal{R} is decreasing function of the frequency. All these limits make sense.

D. Important formulas in full “experimental” notations

The frequencies of the \pm ESR modes given by Eq. (S.46) are:

$$h\nu_{\pm}(0, H, D) = g\mu_B H + \frac{\delta}{1-\delta} g\mu_B H \pm \sqrt{\left(\frac{\delta}{1-\delta} g\mu_B H\right)^2 + (1-\delta^2)\left(\frac{\pi}{2} D\right)^2}. \quad (\text{S.61})$$

The corresponding intensities (S.48) are:

$$A_{\pm}(0, H, D) = \frac{\chi_-}{g\mu_B} \left\{ g\mu_B H \pm \frac{(\pi D/2)^2 - (g\mu_B H)^2 \delta / (1-\delta)}{\sqrt{\left(\frac{\delta}{1-\delta} g\mu_B H\right)^2 + \left(\frac{\pi}{2} D\right)^2}} \right\}, \quad (\text{S.62})$$

with spin susceptibility $\chi_- = g\mu_B/\pi^2 a J(1-\delta)$, and the absorbed power per unit length is given as $I = \frac{(\pi g\mu_B)^2}{\hbar} H_{\text{rad}}^2 \nu A$.

Finally, the mode intensity ratio (S.60) at a given frequency ν is given by

$$\mathcal{R} = \frac{I_{\nu}^{+-}(H_+)}{I_{\nu}^{+-}(H_-)} = \frac{\sqrt{(\delta h\nu)^2 + (1-\delta^2)^2(\pi D/2)^2} - \delta h\nu}{\sqrt{(\delta h\nu)^2 + (1-\delta^2)^2(\pi D/2)^2} + \delta h\nu}. \quad (\text{S.63})$$

V. RENORMALIZATION GROUP RESULTS

Backscattering interaction constant u flows under RG transformation as (remember that $2\delta = u/(2\pi v_F)$)

$$2\delta(\ell) = \frac{2\delta(0)}{1 + 2\delta(0)\ell} \quad (\text{S.64})$$

where $\delta(0) = u(0)/(4\pi v_F)$ is its initial value at the lattice scale and $\ell = \ln(J/E)$ is the logarithmic RG scale, where exchange J serves as the high-energy (lattice scale) cut-off and E is the running energy. Without the magnetic field, $\delta(\ell) \rightarrow 1/\ell$ vanishes as energy goes to zero, $E \rightarrow 0$. In the presence of the field, however, this marginally irrelevant flow is terminated at $E = B$, at which the transverse backscattering \hat{V}_1 effectively averages to 0 and the RG flow stops [10]. For energy below this critical value, the coefficient of \hat{V}_2 term is given by the finite constant $u_z \approx 4\pi v_F \delta(\ell_b)$, with $\ell_b = \ln(J/B)$, while that of the transverse term \hat{V}_1 turns to zero, $u_{\perp} \rightarrow 0$. Importantly, at $E = B$ both coupling constants are finite and given by $u(\ell_b) = 4\pi v_F \delta(\ell_b)$ [10]. This is the essence the Kosterlitz–Thouless RG flow for the spin-1/2 chain in magnetic field, see Fig. 6 in [10] and discussion therein. It is this finite and constant $u = u(\ell_b)$ that shows up in our calculation, simply because we are studying dynamic response of the spin chain at the Zeeman energy B , and not at $E \approx 0$ as is often done when one considers the response at the lowest possible energy.

In a remarkable paper [11] Lukyanov has solved exact RG equations for the running coupling u as function of both temperature T and magnetic field B . According to his Eq. (3.1) his magnetic field h corresponds to our B as $h/2 \rightarrow B$. Also, his $2J$ is our J , see also Eq. (4.5) in [6]. With these simple changes his key result, Eq. (3.18), can be written in our notations as

$$\frac{1}{2\delta} + \frac{1}{2} \ln(2\delta) = -\text{Re}[\psi(1 + i\frac{B}{2\pi T})] + \ln\left(\sqrt{\frac{\pi}{2}} e^{1/4} \frac{J}{T}\right), \quad (\text{S.65})$$

where $\psi(x) = \Gamma'(x)/\Gamma(x)$ is the digamma function and prime denotes derivative with respect to the argument. Asymptotic expansion of digamma function is $\psi(x) \rightarrow \ln(x) - 1/(2x)$ for $x \rightarrow \infty$. Also, $\psi(1) = -\gamma \approx -0.577$, γ is the Euler constant.

Without the magnetic field, $B = 0$, (S.65) becomes

$$\frac{1}{2\delta} + \frac{1}{2} \ln(2\delta) = \ln\left(\sqrt{\frac{\pi}{2}} e^{\gamma+1/4} \frac{J}{T}\right) \quad (\text{S.66})$$

which is Eq. (4.5) in [6].

At zero temperature, $T \rightarrow 0$, we instead use asymptotics of digamma function to find

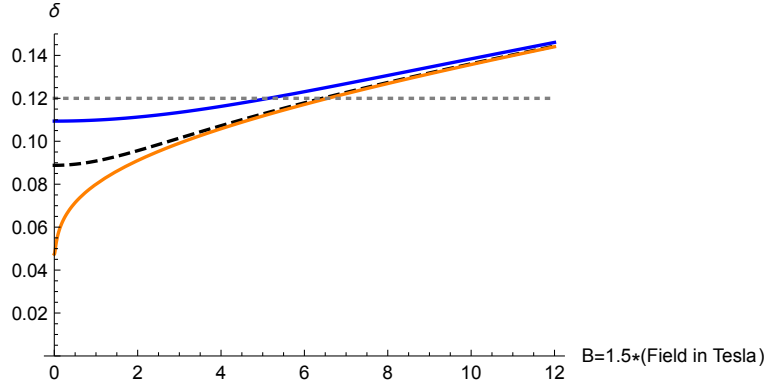
$$\frac{1}{2\delta} + \frac{1}{2} \ln(2\delta) = \ln \left(\sqrt{\frac{\pi}{2}} e^{1/4} \frac{2\pi J}{B} \right). \quad (\text{S.67})$$

Remarkably, T under the logarithm cancels out and is replaced by B . This is of course just the behavior described qualitatively above — the magnetic field cuts RG flow of the backscattering interaction. Notice that up to the relatively small logarithmic correction due to $\ln(2\delta)$ in the left-hand-side of (S.67), this solution is just $2\delta \approx 1/\ln(\text{const} \times J/B)$, just as described above. But the exact solution determines both the constant under the log and corrections to this simple inverse log behavior.

It is easy to solve (S.65) numerically using Mathematica's built-in digamma function. Doing so it is also easy to find that with the excellent accuracy combined effect of T and H can be accounted for by the simple interpolation $T \rightarrow \sqrt{T^2 + e^{2\gamma}(B/(2\pi))^2}$ in (S.66). That is, solving

$$\frac{1}{2\delta} + \frac{1}{2} \ln(2\delta) = \ln \left(\sqrt{\frac{\pi}{2}} e^{\gamma+1/4} \frac{J}{\sqrt{T^2 + \left(\frac{e^\gamma}{2\pi} B\right)^2}} \right) \quad (\text{S.68})$$

one finds $\delta(T, H)$.



SUPP. FIG. 3. Solution of Eq.(S.65) for $T = 1.3\text{K}$ (solid blue line), $T = 0.5\text{K}$ (dashed black line) and $T = 0.0005\text{K}$ (solid orange line) as a function of field B from 0 to 8 T. The field is converted into Kelvins by $B = 1.5 \times (\text{field in Tesla})\text{K}$. Dotted gray line shows $\delta = 0.12$.

Important lesson of this Figure is that finite temperature T cuts the flow of δ to zero. For a field of $g\mu_B H = 6\text{ K}$, which is ~ 4 Tesla, the difference between δ at $T = 1.3\text{ K}$ and $T = 0.5\text{ K}$ is really tiny.

VI. BRIEF SUMMARY OF THE $\mathbf{H} \perp \mathbf{D}$ CASE

When the field \mathbf{H} is applied perpendicular to the DM, there is only one ESR frequency of magnitude $h\nu = \sqrt{(g\mu_B H)^2 + (\pi D/2)^2}$, which corresponds to the total magnetic field experienced by spinons in this geometry. This prediction of the theory is fully supported by our data [12].

VII. ADDITIONAL PHYSICAL CONSEQUENCES OF THE BACKSCATTERING INTERACTION

It is useful to get some additional intuition about the backscattering interaction u . Here we present a calculation of the spinon spin-flip scattering time, following an estimate in [13]. Consider a right-moving spinon with momentum p and spin $s = \uparrow$. Spin-flip part of u (one proportional to $J_R^+ J_L^-$) will cause it to flip a spin to the opposite, spin \downarrow . Mathematically, this spin-flip scattering time is given by the imaginary part of the (retarded) self-energy in the diagram in Fig. 4,

$$\frac{\hbar}{\tau} = 2 \text{Im} \Sigma^R(\epsilon = v_F p, p), \quad (\text{S.69})$$

where the self-energy is to be evaluated on the mass-shell, i.e. for $\epsilon = v_F p$. We start by writing the self-energy in the Matsubara formalism

$$\Sigma(\epsilon_n, p) = -(u/2)^2 T \sum_{\epsilon'_m} \int \frac{dp_1}{2\pi} G(\epsilon'_m, p_1) \Pi(\epsilon_n - \epsilon'_m, p - p_1) \quad (\text{S.70})$$

where ϵ 's are fermion (odd) Matsubara frequencies. We use spectral representation

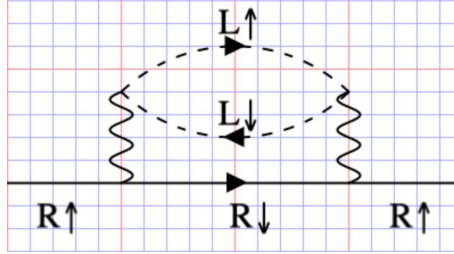
$$G(\epsilon'_m, p_1) = \int_{-\infty}^{\infty} \frac{dx}{\pi} \frac{\text{Im}G^R(x, p_1)}{x - i\epsilon'_m} \quad (\text{S.71})$$

and similar for the polarization bubble $\Pi(\epsilon_n - \epsilon'_m, p - p_1)$ of the left-moving spinons. This gives us

$$\Sigma(\epsilon_n, p) = -(u/2)^2 \int \frac{dp_1}{2\pi} \int_{-\infty}^{\infty} \frac{dx}{\pi} \frac{dy}{\pi} \text{Im}G^R(x, p_1) \text{Im}\Pi^R(y, p - p_1) S_1, \quad (\text{S.72})$$

where

$$S_1 = T \sum_{\epsilon'_m} \frac{1}{x - i\epsilon'_m} \frac{1}{y - i\epsilon_n + i\epsilon'_m}. \quad (\text{S.73})$$



SUPP. FIG. 4. Self-energy diagram describing interaction of the right-moving spinons with the left-moving ones. Wiggly lines represent interaction u . Its imaginary part gives spinon scattering rate $1/\tau$.

This sum is evaluated by breaking into elementary fractions and using

$$T \sum_{\epsilon'_m} \frac{1}{x - i\epsilon'_m} = T \sum_{m=-\infty}^{\infty} \frac{x}{x^2 + (\pi T(2m+1))^2} = \frac{1}{2} \tanh(x/2T) = \frac{1}{2} - n_F(x), \quad (\text{S.74})$$

where $n_F(x) = 1/(e^{\beta x} + 1)$ is the Fermi distribution function. Next, we see that $\omega_n = \epsilon_n - \epsilon'_m \rightarrow 2\pi n T$ is Bose (even) frequency and

$$T \sum_{\omega_n} \frac{1}{y - i\omega_n} = T \sum_{n=-\infty}^{\infty} \frac{y}{y^2 + (2\pi T n)^2} = \frac{T}{y} + 2T \sum_{n=1}^{\infty} \frac{y}{y^2 + (2\pi T n)^2} = \frac{1}{2} \coth(y/2T) = \frac{1}{2} + n_B(y), \quad (\text{S.75})$$

where $n_B(y) = 1/(e^{\beta y} - 1)$ is the Bose distribution function.

This leads to

$$\Sigma(\epsilon_n, p) = -(u/2)^2 \int \frac{dp_1}{2\pi} \int_{-\infty}^{\infty} \frac{dx}{\pi} \frac{dy}{\pi} \text{Im}G^R(x, p_1) \text{Im}\Pi^R(y, p - p_1) \frac{1 - n_F(x) + n_B(y)}{x + y - i\epsilon_n}, \quad (\text{S.76})$$

which is easy to continue to the real frequency $i\epsilon_n \rightarrow \epsilon + i0$, thereby obtaining the retarded self-energy $\Sigma(\epsilon_n, p) \rightarrow \Sigma^R(\epsilon, p)$. We need the imaginary part of that,

$$\text{Im}\Sigma^R(\epsilon, p) = -\frac{(u/2)^2}{\pi} \int_{-\infty}^{\infty} dx dy \delta(\epsilon - x - y) \text{Im}G^R(x, p_1) \text{Im}\Pi^R(y, p - p_1) [1 - n_F(x) + n_B(y)]. \quad (\text{S.77})$$

To obtain the imaginary part of the left-spinon bubble $\Pi^R(y, p - p_1)$ we start with its Matsubara expression

$$\Pi(\omega_n, k) = -T \sum_{\epsilon_n} \int \frac{dp_2}{2\pi} G(\epsilon_n, p_2) G(\epsilon_n - \omega_n, p_2 - k) = -T \sum_{\epsilon_n} \int \frac{dp_2}{2\pi} \frac{1}{i\epsilon_n + v_F p_2} \frac{1}{i\epsilon_n - i\omega_n + v_F p_2 - v_F k}. \quad (\text{S.78})$$

This too is broken into elementary fractions and, with the help of (S.74), is brought into a form

$$\Pi(\omega_n, k) = \int \frac{dp_2}{2\pi} \frac{n_F(v_F p_2 - v_F k) - n_F(v_F p_2)}{i\omega_n + v_F k}, \quad (\text{S.79})$$

which is easy to analytically continue $\omega_n \rightarrow \omega + i0$ and obtain

$$\text{Im}\Pi^R(\omega, k) = -\pi \int \frac{dp_2}{2\pi} \delta(\omega + v_F k) [n_F(v_F p_2 + \omega) - n_F(v_F p_2)]. \quad (\text{S.80})$$

Plugging (S.80) into (S.77), using $\text{Im}G^R(x, p_1) = -\pi\delta(x - v_F p_1)$ and then integrating over x , followed by integration over y , we obtain [also use $n_B(-z) = -(1 + n_B(z))$]

$$\text{Im}\Sigma^R(\epsilon, p) = \pi(u/2)^2 \int \frac{dp_1}{2\pi} \frac{dp_2}{2\pi} \delta(\epsilon + v_F(p - p_1) - v_F p_1) [n_F(v_F p_1) + n_B(v_F(p - p_1))] [n_F(v_F p_2 - v_F(p - p_1)) - n_F(v_F p_2)]. \quad (\text{S.81})$$

We see that on the mass-shell $\epsilon = v_F p$ the argument of the delta-function reduces to $2v_F(p - p_1)$, which leads to the divergence of the Bose function $n_B(v_F(p - p_1)) \rightarrow T/(v_F(p - p_1))$. But at the same time the last square bracket reduces to the derivative $n_F(v_F p_2 - v_F(p - p_1)) - n_F(v_F p_2) \rightarrow \beta v_F(p - p_1) e^{\beta\epsilon} / (e^{\beta\epsilon} + 1)^2$, with $\epsilon = v_F p_2$. Taking this limit carefully we observe that in the $p \rightarrow p_1$ limit $n_B(v_F(p - p_1)) [n_F(v_F p_2 - v_F(p - p_1)) - n_F(v_F p_2)] \rightarrow e^{\beta v_F p_2} / (e^{\beta v_F p_2} + 1)^2$, so that

$$\text{Im}\Sigma^R(v_F p, p) = \frac{(u/2)^2}{4v_F} \int_{-\infty}^{\infty} \frac{dp_2}{2\pi} \frac{e^{\beta v_F p_2}}{(e^{\beta v_F p_2} + 1)^2} = T \frac{u^2}{32\pi v_F^2}. \quad (\text{S.82})$$

Therefore, using $\delta = u/(4\pi v_F)$, we get the final result

$$\frac{\hbar}{\tau} = \pi\delta^2 T. \quad (\text{S.83})$$

Next, the mean-free path of the spin- \uparrow spinon can be estimated as

$$\ell = v_F \tau = \frac{\hbar v_F}{\pi\delta^2 T} \approx \frac{35Ja}{T}, \quad (\text{S.84})$$

where $\delta = 0.12$ was used. Thus, for a chain with $J = 20$ K, we have that $\ell/a = 700/T$. The mean-free path is about 700 lattice spacings at $T = 1$ K. This is huge. We see again that even although u is quite large, what really matters is δ , which is quite small.

We note that (S.83) can be also obtained from the simple Fermi's golden rule calculation, similar to how it was done in [13]. The initial state is $|i\rangle = \psi_{R,\uparrow}^\dagger(p)|0\rangle$, while the final state $|f\rangle = \psi_{R,\downarrow}^\dagger(p_1)\psi_{L,\uparrow}^\dagger(p_2 + p - p_1)\psi_{L,\downarrow}(p_2)|0\rangle$ involves a particle-hole pair of the left-movers with opposite spins. Using

$$\frac{1}{\tau} = \frac{2\pi}{\hbar} \sum_f |\langle f | \hat{V}_{\text{bs}} | i \rangle|^2 \delta(E_f - E_i) \delta(P_f - P_i), \quad (\text{S.85})$$

one recovers result (S.83).

VIII. EXPERIMENTAL INFORMATION

A. Samples

The monocrystalline samples of $K_2CuSO_4Br_2$ with typical masses of 10 – 20 mg were grown at ETH Zürich from aqueous solution according to the techniques described in detail in Refs. [14, 15]. The crystals are transparent and dark brownish-green in color. They have forms of rectangular or rhombic prisms elongated along the chain b direction. The orientation of the samples was checked with Bruker APEX-II single crystal diffractometer.

B. ESR experiments

The experiments were done at the Kapitza Institute on a set of multifrequency (1-250 GHz) resonant cavity ESR inserts into ^3He -pumping cryostat with a 14 T cryomagnet and a ^4He -pumping cryostat with a 6 T magnet. In either case the sample was mounted into the copper resonator with $\mathbf{H} \parallel \mathbf{b}$ in the location, where the maximum of oscillating magnetic field is expected. The transmission of microwave power through the sample-containing resonator was measured as the function of the magnetic field at a fixed frequency ν . At a frequency corresponding to the resonator mode, amplification of the sensitivity of about resonator factor $Q \sim 10^3 - 10^4$ may be achieved in comparison with measuring transmission through a waveguide with the same sample. Also, the microwave source signal was amplitude-modulated at frequency of few kHz (to allow the lock-in detection scheme) and frequency-modulated around ν (with depth of 100 MHz typically) to avoid detuning effects due to the change in the reactive sample's susceptibility part at the resonance.

In general, for small sample absorption the transmitted power can be approximated as:

$$P(H) = P_0 \left[1 - 4\pi Q \eta \frac{V_{\text{sample}}}{V_{\text{resonator}}} \chi''(q = 0, \nu, H) \right], \quad (\text{S.86})$$

where P_0 would correspond to the power transmitted through the unloaded resonator (i.e. far away from the susceptibility peak), and Q is the quality factor of the particular cavity eigenfrequency ν , η is a geometrical factor of the order of 1. Also the ratio of sample and resonator volumes plays a role. The dissipative part of susceptibility χ'' here is defined per unit volume. Thus, in the ESR experiment of this type we directly probe the field dependence of the dissipative part of uniform susceptibility at a given frequency, although without no absolute calibration in general (thanks to a number of frequency- and geometry-related factors in (S.86)). Also, in the case of *strong* sample absorption the non-linear generalization of (S.86) needs to be used:

$$P(H) = P_0 \frac{1}{\left(1 + 2\pi \eta Q \frac{V_{\text{sample}}}{V_{\text{resonator}}} \chi''(q = 0, \nu, H) \right)^2}. \quad (\text{S.87})$$

In our case this may be crucial in order to correctly estimate the ESR line intensities as we will discuss below.

C. Fitting the line profiles

A typical ESR line can be conveniently described by a single Lorentzian profile:

$$\mathcal{L}(H, H_0, \Gamma_{1/2}, \mathcal{A}) = \frac{\mathcal{A}}{1 + \left(\frac{H - H_0}{\Gamma_{1/2}} \right)^2} \quad (\text{S.88})$$

Here the parameters are the line amplitude \mathcal{A} , half-width at half-maximum $\Gamma_{1/2}$, and the resonance field H_0 . Clearly, while the determination of the resonance field does not require distinguishing between the linear and non-linear approaches (S.86, S.87), for large line amplitudes the latter is needed in order to get the resonance integral intensity $I = \pi \mathcal{A} \Gamma_{1/2}$ correctly.

In the present case we deal with multiple overlapping lines. Hence, at each frequency we approximate the quantity of interest

$$2\pi Q\eta \frac{V_{\text{sample}}}{V_{\text{resonator}}} \chi''(q=0, \nu, H) = \sum_i \mathcal{L}(H, H_0^{(i)}, \Gamma_{1/2}^{(i)}, \mathcal{A}^{(i)}) + \mathcal{L}(H, -H_0^{(i)}, \Gamma_{1/2}^{(i)}, \mathcal{A}^{(i)}) \quad (\text{S.89})$$

with a number of independent ESR modes i (up to 3 in our case). An effect of the resonance at the oppositely directed magnetic field (that may be important for broad lines with small resonant fields), which corresponds to a second circular polarized component of a linearly polarized microwave field is explicitly accounted for. Examples of such multi-line fits can be found in Fig. 2c of the main text. Thus, the mode intensities $I^+ = \pi \mathcal{A}^+ \Gamma_{1/2}^+$ and $I^- = \pi \mathcal{A}^- \Gamma_{1/2}^-$ that we would determine from the fit, would be proportional to the calculated spectral weights A^+ , A^- (S.48). Using the *intensity ratio* at the given frequency instead allows us to completely eliminate the uncalibrated prefactors like Q etc from the description. The observed intensity ratio I^+/I^- obtained from the fit can be directly compared to the parameter-free theoretical description (S.60).

[1] Daniel P. Arovas and Assa Auerbach, “Functional integral theories of low-dimensional quantum Heisenberg models,” *Phys. Rev. B* **38**, 316–332 (1988).

[2] Daniel C. Dender, *Spin dynamics in the quasi-one-dimensional S=1/2 Heisenberg antiferromagnet copper benzoate*, Ph.D. thesis, Johns Hopkins University, Baltimore, Maryland (1997), uMI Number: 9821113.

[3] D. C. Dender, P. R. Hammar, Daniel H. Reich, C. Broholm, and G. Aeppli, “Direct Observation of Field-Induced Incommensurate Fluctuations in a One-Dimensional $S = 1/2$ Antiferromagnet,” *Phys. Rev. Lett.* **79**, 1750–1753 (1997).

[4] Hamed Karimi and Ian Affleck, “Transverse spectral functions and Dzyaloshinskii-Moriya interactions in XXZ spin chains,” *Phys. Rev. B* **84**, 174420 (2011).

[5] A. Keselman, L. Balents, and O. A. Starykh, “Dynamical Signatures of Quasiparticle Interactions in Quantum Spin Chains,” *Phys. Rev. Lett.* **125**, 187201 (2020).

[6] Ion Garate and Ian Affleck, “Interplay between symmetric exchange anisotropy, uniform Dzyaloshinskii-Moriya interaction, and magnetic fields in the phase diagram of quantum magnets and superconductors,” *Phys. Rev. B* **81**, 144419 (2010).

[7] K. Yu. Povarov, A. I. Smirnov, O. A. Starykh, S. V. Petrov, and A. Ya. Shapiro, “Modes of Magnetic Resonance in the Spin-Liquid Phase of Cs_2CuCl_4 ,” *Phys. Rev. Lett.* **107**, 037204 (2011).

[8] Yang-Hao Chan, Wen Jin, Hong-Chen Jiang, and Oleg A. Starykh, “Ising order in a magnetized Heisenberg chain subject to a uniform Dzyaloshinskii-Moriya interaction,” *Phys. Rev. B* **96**, 214441 (2017).

[9] A.O. Gogolin, A.A. Nersesyan, and A.M. Tsvelik, *Bosonization and Strongly Correlated Systems* (Cambridge University Press, 2004).

[10] Ian Affleck and Masaki Oshikawa, “Field-induced gap in Cu benzoate and other $S = \frac{1}{2}$ antiferromagnetic chains,” *Phys. Rev. B* **60**, 1038–1056 (1999).

[11] Sergei Lukyanov, “Low energy effective Hamiltonian for the XXZ spin chain,” *Nuclear Physics B* **522**, 533–549 (1998).

[12] A. I. Smirnov, T. A. Soldatov, K. Yu. Povarov, M. Hälg, W. E. A. Lorenz, and A. Zheludev, “Electron spin resonance in a model $S = \frac{1}{2}$ chain antiferromagnet with a uniform Dzyaloshinskii-Moriya interaction,” *Phys. Rev. B* **92**, 134417 (2015).

[13] L. Balents and R. Egger, “Spin-dependent transport in a Luttinger liquid,” *Phys. Rev. B* **64**, 035310 (2001).

[14] M. Hälg, W. E. A. Lorenz, K. Yu. Povarov, M. Måansson, Y. Skourski, and A. Zheludev, “Quantum spin chains with frustration due to Dzyaloshinskii-Moriya interactions,” *Phys. Rev. B* **90**, 174413 (2014).

[15] M. Hälg, *Quantum Criticality, Universality and Scaling in Organometallic Spin-Chain Compounds* (PhD thesis, ETH Zürich, 2015).